



A past and present perspective on the European summer vapour pressure deficit

5 Viorica Nagavciuc^{1,2 *†}, Simon L. L. Michel^{3†}, Daniel F. Balting^{1†}, Gerhard Helle⁴, Mandy Freund⁵,
Gerhard H. Schleser⁶, David N. Steger⁷, Gerrit Lohmann^{1,8} and Monica Ionita^{1,2,9}

¹Alfred-Wegener-Institute, Bremerhaven, 27570, Germany

²Faculty of Forestry, Ștefan cel Mare University, Suceava, 720229, Romania

³Institute for Marine and Atmospheric research Utrecht (IMAU), Department of Physics, Utrecht University, Utrecht, Netherlands

10 ⁴German Research Centre for Geosciences, Potsdam, 14473, Germany

⁵Climate and Energy College, University of Melbourne, Melbourne, VIC 3010, Australia

⁶Institute of Bio- and Geosciences IBG-3, Forschungszentrum Jülich, Jülich 52428, Germany

⁷University of Basel, Department of Environmental Sciences, Basel, 4056, Switzerland

⁸Physics Department, University of Bremen, Bremen, 28359, Germany

15 ⁹Emil Racovita Institute of Speleology, Romanian Academy, Cluj-Napoca, 400006, Romania

*Correspondence to: Viorica Nagavciuc (viorica.nagavciuc@awi.de)

†Equally contributing co-authors

20 **Abstract.** The response of evapotranspiration to anthropogenic warming is of critical importance for the water and carbon
cycle. Contradictory conclusions about evapotranspiration changes are caused primarily by their brevity in time and sparsity
in space, as well as the strong influence of internal variability. Here, we present the first gridded reconstruction of the summer
vapour pressure deficit (VPD) for the past four centuries at the European level. This gridded reconstruction is based on 26
European tree-ring oxygen isotope records and is obtained using a Random Forest approach. Based on our reconstruction, we
25 show that from the mid- 1700s, a trend towards higher VPD occurred in Central Europe and the Mediterranean region which
is related to a simultaneous increase in temperature and decrease in precipitation. This increasing VPD trend continues
throughout the observational period and in recent times. Moreover, our VPD reconstruction helps to visualize the local and
regional impacts of the current climate change as well as to minimize statistical uncertainties of historical VPD variability.
Furthermore, the interdisciplinary use of the data should be emphasized, as VPD is a crucial parameter for many climatological
30 feedback processes in the earth surface system. The reconstructed VPD gridded data, over the last 400 years, is available at
the following link: <https://doi.org/10.5281/zenodo.5958836> (Balting, D. F. et al., 2022).



1. Introduction

Evapotranspiration is a critical factor for understanding the links and feedback between atmospheric CO₂ and global climate (Good et al., 2015; IPCC, 2021b, 2021a). Within the terrestrial water fluxes, vegetation-produced transpiration represents the dominant factor (Good et al., 2015; Jasechko et al., 2013). One key driver for such vegetation resources and dynamics is vapor pressure deficit (VPD), defined by the difference between the water vapor pressure at saturation and the actual water vapor pressure (Grossiord et al., 2020; Lawrence, 2005). The VPD represents the atmospheric evaporative demand which has an influence on the leaf-level transpiration of terrestrial vegetation and the corresponding stomatal conductance (Grossiord et al., 2020). With increasing VPD, the stomata closes to minimize water loss (Running, 1976) due to the high atmospheric evaporative demand. Consequently, a minimal stomata opening decreases stomatal conductance and photosynthetic activity (Fletcher et al., 2007). Extremely high VPD may even lead to reduced growth, a higher risk of carbon starvation, and hydraulic failure (Grossiord et al., 2020). In contrast, low VPD leads to reduced water transport into the leaves and thus a reduced supply of nutrients. Therefore, VPD is an important factor for plant activity (Novick et al., 2016), notably affecting plant growth (Restaino et al., 2016), forest mortality (Williams et al., 2013), drought occurrence (Dai, 2013), crop production (Zhao et al., 2017) and wildfire occurrence (Seager et al., 2015), among others.

Since VPD is a function of temperature (Lawrence, 2005), the effects of climate change and the associated increase in the mean global temperature lead to positive trends in the regional and global VPD (Grossiord et al., 2020; IPCC, 2021b). For instance, studies have shown that the VPD has been increasing sharply at a global scale since the year 2000 (Simmons et al., 2010; Willett et al., 2014; Yuan et al., 2019). Spatially explicit VPD records derived from remote sensing data cover only the last ~50 years and vary in quality, so long-term perspectives of VPD variability are lacking. However, long-term perspectives can help to put recently observed trends of VPD in a long-term context relevant for estimating the significance and robustness of these changes both at local as well as at the continental scales. Furthermore, it is essential to investigate the independent physiological effects of VPD on large-scale vegetation dynamics, a topic which is far less explored (Grossiord et al., 2020). So far, the first local reconstruction studies have shown the potential for a long-term perspective on VPD (Liu et al., 2017; Roibu et al., 2022). Churakova Sidorova et al., (2020) have shown that the recent VPD increase does not yet exceed the maximum values reconstructed during the Medieval Warm Anomaly in Siberia. Nevertheless, most studies lack a wider spatial perspective as they only reconstruct VPD time series for a single location. Therefore, appears the necessity for high resolution VPD reconstructions over extended spatial regions (e.g. the European region).

Tree-ring sequences are one of the most used proxy archives for paleoclimatic reconstruction because of their annual resolution, precise dating, and widespread spatial extent (Leonelli et al., 2017). Moreover, they allow us to create chronologies of thousands of years and give us the possibility to explore the climate through different tree ring based climate-sensitive parameters, such as: tree-ring width, maximum density, and/or stable isotopes (Nagavciuc et al., 2022). Of all physical or chemical parameters to be measured of annual rings, the stable oxygen isotope ratio of tree-ring cellulose ($\delta^{18}\text{O}$) has the advantage that the isotopic fractions controlled by physiological processes are reasonably well understood and the



70 statistical relationship with climatic and environmental quantities is rather robust (McCarroll and Loader, 2004). Combining
these advantages with the advantages of annual tree rings, tree ring- $\delta^{18}\text{O}$ may be one of the most valuable proxies for the
paleoclimatic reconstructions. Nonetheless, there are still questions to be answered about the variability of $\delta^{18}\text{O}$ in the arboreal
system (Gagen et al., 2022). To a good approximation, tree ring- $\delta^{18}\text{O}$ from European sites can be considered as a combined
75 enrichment of leaf water controlled by leaf-to-air VPD, so that tree ring- $\delta^{18}\text{O}$ can be used as a proxy for variations in VPD
(Ferrio and Voltas, 2005; Kahmen et al., 2011).

In order to have a long-term overview of the observed changes and trends in the regional and global VPD, one needs
to look back in the past, by employing different proxy indicators (e.g. from tree rings). In this respect, the availability of the
ISONET network (Balting et al., 2021; ISONET Project Members et al., 2023; Treydte et al., 2007a, 2007b) gave us the
80 opportunity to develop for the first VPD reconstruction at the European level, by using multiple stable oxygen isotope records
derived from tree-rings. The reconstruction of our VPD dataset, which covers the last 400 years, has been obtained by
applying a Random Forest (RF) regression method (Breiman, 2001). According to Yang et al., (2020), RF has become one
of the most successful machine learning algorithms for practical applications over the last two decades due to its proven
accuracy, stability, speed of processing, and ease of use (Bair et al., 2018; Belgiu and Drăgu, 2016; Maxwell et al., 2018; Qu
85 et al., 2019; Reichstein et al., 2019; Rodriguez-Galiano et al., 2012; Tyralis et al., 2019). The term RF describes a non-linear
and robust technique in which several decision trees are built and aggregated at the end to make predictions or perform
reconstructions (Breiman, 2001). The RF approach is increasingly applied in climate and environmental sciences, and has
been used for the prediction of snow depth (Yang et al., 2020), solar radiation (Prasad et al., 2019), daily ozone (Zhan et al.,
2018), precipitation (Ali et al., 2020); as well as for reconstructions of last millennium North Atlantic Oscillation (Michel
90 et al., 2020), Atlantic Multidecadal Variability (Michel et al., 2022), El Niño Southern Oscillation (Delcroix et al., 2022),
streamflow since 1485 C.E. (Li et al., 2019) and vegetation cover during the mid-Holocene and the Last Glacial Maximum
(Lindgren et al., 2021), as well as for tree growth response to earthquakes (Mohr et al., 2021). Although RF models have
proved to be a useful method in geosciences, studies on the spatial-temporal reconstruction of climate variables based on
 $\delta^{18}\text{O}$ are relatively rare due to the low availability of $\delta^{18}\text{O}$ time series.

95 The purpose of this study is to apply a RF approach (Breiman, 2001) for reconstructing the European summer VPD
for the first time, from a proxy network that is based on 26 series of tree-ring $\delta^{18}\text{O}$ and covers the period 1600-1994 (Balting
et al., 2021; ISONET Project Members et al., 2023). The main aim is to present the summer VPD reconstruction dataset for
the last 400 years over Europe and provide both a spatial as well as a temporal long-term perspective on the past summer
VPD variability. The VPD reconstruction is analyzed subsequently from a spatio-temporal perspective for Northern Europe,
100 Central Europe, and Mediterranean regions (Iturbide et al., 2020) as defined and used in the Sixth Assessment Report (AR6)
of the IPCC (IPCC, 2021a). The data evaluation in this paper is structured as follows: in Section 2 we give a detailed
description of the data and methods employed, while the main results are presented in Section 3: first, we present the **climate**
sensitivity of $\delta^{18}\text{O}$ for VPD variability and the validations statistics for the reconstruction; second, we investigate the spatial



105 variability of VPD in comparison with other studies and analyses for selected extreme years, for additional validation of our
reconstructions. Uncertainties are discussed in Section 4, while conclusions and outlooks are presented in Section 5. In this
way, the past and present VPD conditions are presented and evaluated to assess the statistical significance of observed trends
to understand VPD variability on a local, regional, and continental scale.

2. Sample sites and used climate data

110 2.1 The stable isotope network

To reconstruct the European summer VPD, we used 26 time series of stable oxygen isotopes in tree-ring cellulose ($\delta^{18}\text{O}$)
(Figure 1, Table 1). From the 26 time series used in this study, 21 time series were obtained from the dataset generated by the
EU project ISONET (EVK2-CT-2002-00147) (Balting et al., 2021; ISONET Project Members et al., 2023; Treydte et al.,
2007a, 2007b). In addition to the ISONET dataset, we added five new $\delta^{18}\text{O}$ time series from Bulgaria, Turkey, southwestern
115 Germany, Romania, and Slovenia (Hafner et al., 2014; Heinrich et al., 2013; Nagavciuc et al., 2019) (Figure 1).

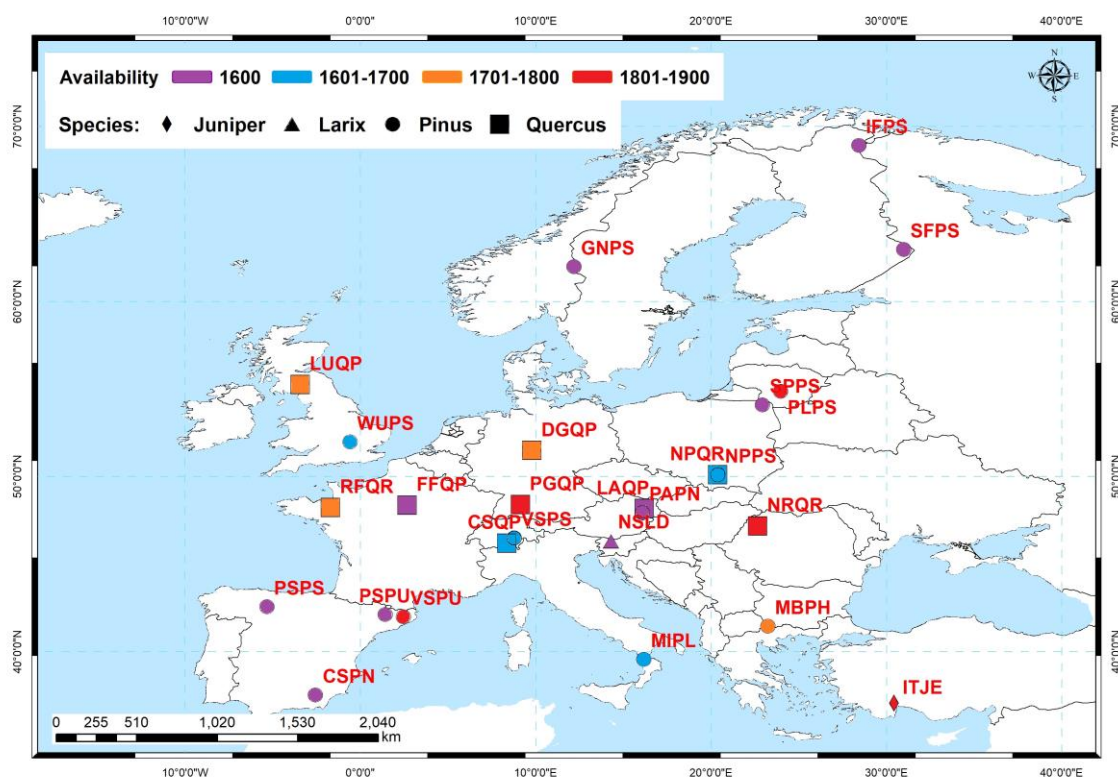
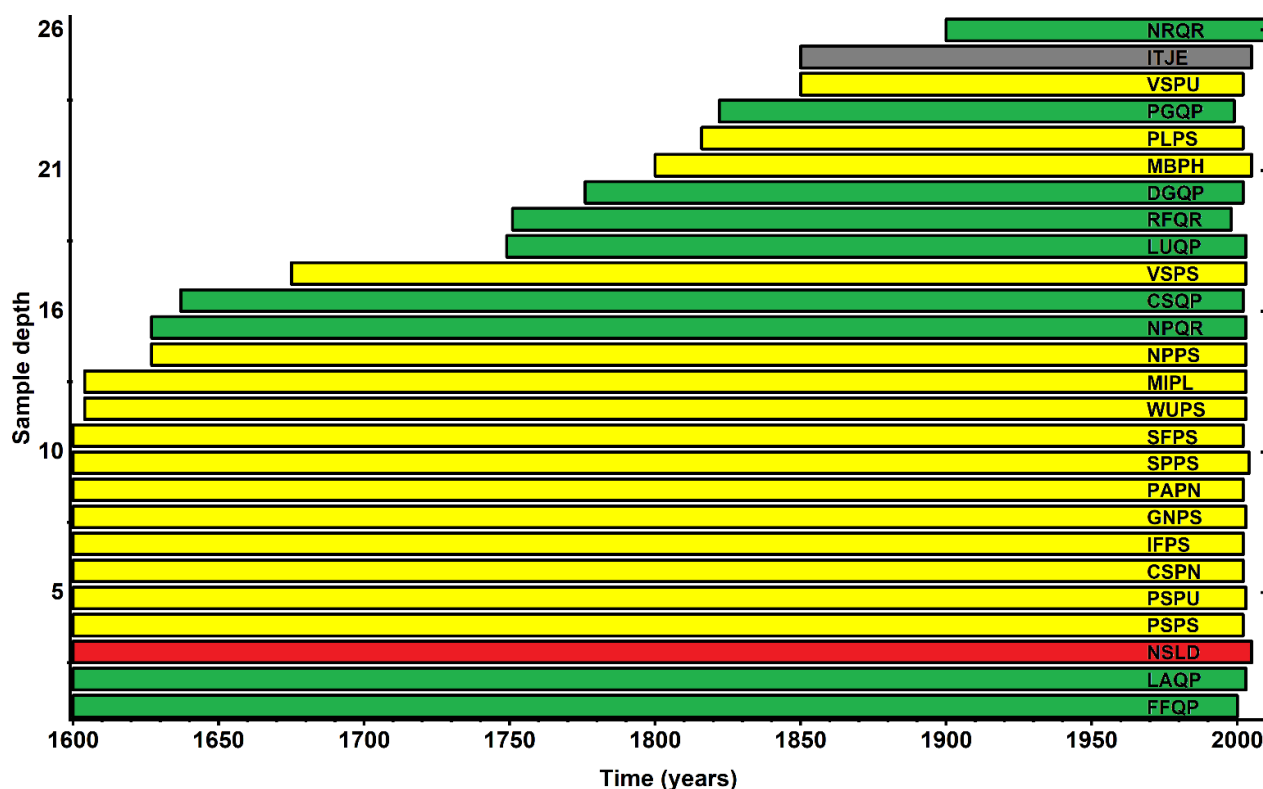


Figure 1: The site distribution of the used $\delta^{18}\text{O}$ network combined with the corresponding tree genera



120 The detailed measurement methodologies used within the ISONET project as well as for the other sites are described in the
description file of the data set (ISONET Project Members et al., 2023) and, in more detail, in the previously published papers
(Boettger et al., 2007; Hafner et al., 2014; Heinrich et al., 2013; Nagavciuc et al., 2019; Treydte et al., 2007b, 2007a). At least
four dominant trees were selected at each site and two increment cores were taken per tree for the ISONET project; 15 cores
of five living trees were taken from the site in Turkey (Heinrich et al., 2013), 12 trees were sampled for the Slovenian time
125 series (Hafner et al., 2014) and from nine trees, one core per tree was taken in Romania (Nagavciuc et al., 2019). A standard
dendrochronological dating method was performed (Fritts, 1976), and subsequent individual growth rings were dissected from
the cores. All tree rings from the same year were pooled for most sites prior to cellulose extraction for the ISONET sites
(Treydte et al., 2007b, 2007a) as well as for the Romanian site (Nagavciuc et al., 2019). The dissected tree rings from the
Slovenian and Turkish sites were measured individually and not pooled (Hafner et al., 2014; Heinrich et al., 2013). For oak,
130 only the latewood was used for the analyses. This approach was assumed to use predominantly climate signals from the current
year, as the earlywood of oaks can contain climate information from the previous year (Davies and Loader, 2020; González-
González et al., 2015). The results are expressed using the conventional δ (delta) notation, in per mil (‰) relative to the Vienna
Standard Mean Ocean Water (VSMOW) (Craig, 1957).



135

Figure 2: The number of available $\delta^{18}\text{O}$ time series within the network. The *Quercus* sites are represented with green color, *Pinus* sites with yellow, *Larix* with red, and *Juniperus* with grey. For site codes please see table 1.



140 The isotope network presented here consists of nine deciduous tree sites (*Quercus*) and 17 conifer sites (*Pinus*, *Juniper*, *Larix*; see Table 1). The sample sites are well distributed over Europe (Figure 1). The elevation of the locations varies from 10 m a.s.l. (Woburn, UK) to 2.120 m a.s.l. (Pedraforca, Spain). The longest chronologies cover a period from 1600 to 2005. The highest data density (i.e., 26 time series) is available for the period 1900-1994 (Figure 2). For several sites or regional groups of sites from the ISONET datasets, the data is published within individual studies (Andreu-Hayles et al., 2017; Etien et al., 2008; Haupt et al., 2011; Helama et al., 2014; Hilasvuori et al., 2009; Labuhn et al., 2014, 2016; Rinne et al., 2013; Saurer et al., 2014, 2008, 2012; Vitas, 2008).

145

Table 1: Characteristics of each sample site used within our study. 21 of the 26 $\delta^{18}\text{O}$ records were obtained from the EU project ISONET and five additional sites from Bulgaria, Turkey, Southwest Germany, Romania, and Slovenia

	Code	Location	Country	Species	First year	Last year	Lon.	Lat.	Altitude	Source
1	CSPN	Cazorla	Spain	<i>Pinus nigra</i>	1600	2002	-2.57°	37.53°	1820 m	ISONET
2	CSQP	Cavergno	Switzerland	<i>Quercus petraea</i>	1637	2002	8.36°	46.21°	900 m	ISONET
3	DGQP	Dransfeld	Germany	<i>Quercus petraea</i>	1776	2002	9.78°	51.50°	320 m	ISONET
4	FFQP	Fontainebleau	France	<i>Quercus petraea</i>	1600	2000	2.67°	48.38°	100 m	ISONET
5	GNPS	Gutuli	Norway	<i>Pinus sylvestris</i>	1600	2003	12.18°	62.00°	800 m	ISONET
6	IFPS	Inari	Finland	<i>Pinus sylvestris</i>	1600	2002	28.42°	68.93°	150 m	ISONET
7	ITJE	Isibeli	Turkey	<i>Juniper excelsa</i>	1850	2005	30.45°	37.06°	1800 m	(Heinrich et al., 2013)
8	LAQP	Lainzer Tiergarten	Austria	<i>Quercus petraea</i>	1600	2003	16.20°	48.18°	300 m	ISONET
9	LUQP	Lochwood	United Kingdom	<i>Quercus petraea</i>	1749	2003	-3.43°	55.27°	175 m	ISONET
10	MIPL	Monte Pollino	Italy	<i>Pinus leucodermis</i>	1604	2003	16.16°	39.58°	1900 m	ISONET
11	MBPH	Mount Vichren	Bulgaria	<i>Pinus heldreichii</i>	1800	2005	23.24°	41.46°	1900 m	(Balting et al., 2021)
12	NSLD	Naklo	Slovenia	<i>Larix decidua</i>	1600	2005	14.30°	46.30°	440 m	Hafner
13	NPQR	Niepolomice	Poland	<i>Quercus robur</i>	1627	2003	20.38°	50.12°	190 m	ISONET
14	NPPS	Niepolomice	Poland	<i>Pinus sylvestris</i>	1627	2003	20.38°	50.12°	190 m	ISONET
15	NRQR	Nusfalau	Romania	<i>Quercus robur</i>	1900	2016	22.66°	47.19°	270 m	(Nagavciuc et al., 2019)
16	PLPS	Panemunės	Lithuania	<i>Pinus sylvestris</i>	1816	2002	23.97°	54.88°	45 m	ISONET
17	PSPU	Pedraforca	Spain	<i>Pinus uncinata</i>	1600	2003	1.42°	42.13°	2120 m	ISONET
18	PSPS	Pinar de Lillo	Spain	<i>Pinus sylvestris</i>	1600	2002	-5.34°	42.57°	1600 m	ISONET
19	PGQP	Plieningen	Germany	<i>Quercus petraea</i>	1822	1999	9.13°	48.42°	340 m	(Balting et al., 2021)



21	PAPN	Poellau	Austria	<i>Pinus nigra</i>	1600	2002	16.06°	47.95°	500 m	ISONET
20	RFQR	Rennes	France	<i>Quercus robur</i>	1751	1998	-1.7°	48.25°	100 m	ISONET
22	SFPS	Sivakkovaara	Finland	<i>Pinus sylvestris</i>	1600	2002	30.98°	62.98°	200 m	ISONET
23	SPPS	Suwalki	Poland	<i>Pinus sylvestris</i>	1600	2004	22.93°	54.10°	160 m	ISONET
24	VSPS	Vigera	Switzerland	<i>Pinus sylvestris</i>	1675	2003	8.77°	46.50°	1400 m	ISONET
25	VSPU	Vinuesa	Spain	<i>Pinus uncinata</i>	1850	2002	2.45°	42.00°	720 m	ISONET
26	WUPS	Woburn	United Kingdom	<i>Pinus sylvestris</i>	1604	2003	-0.59°	51.98°	10 m	ISONET

2.2 Climate data

150 Mean air temperature (°C) and relative humidity (%) from the near-surface (i.e., 2m above ground level) were derived from the 20th Century Reanalysis Project (20CR) version V3 (Slivinski et al., 2019) at a monthly resolution. The 20CR reanalysis has a temporal resolution of three hours, 28 different pressure levels, and a resolution of 1° x 1°. We use the ensemble mean derived from an 80-member ensemble. The climate variables are available for the period from 1836 to 2015 and they are provided by NOAA/OAR/ESRL PSL, Boulder, Colorado, USA (https://psl.noaa.gov/data/gridded/data.20thC_ReanV3.html).

155

2.3 General procedure of the European VPD reconstruction

To reconstruct spatially the European summer VPD for the last 400 years we have used the Random Forest method (see Supplement Section 1) (Breiman, 2001). The VPD data derived from 20CRV3 (Slivinski et al., 2019) and the $\delta^{18}\text{O}$ network data were used as input. There is a small number of missing data (0.38% entries in total) which are infilled using an iterative
 160 Principal Component Analysis approach following Josse and Husson, (2016). For each grid point of the observations, sensitivity tests are performed prior to the reconstruction, where only $\delta^{18}\text{O}$ data significantly correlated at the 95% confidence level with the observed VPD are considered. These tests are carried out with a correction of the degrees of freedom using first order autocorrelation coefficients estimated from both timeseries as in Michel et al., (2020).

The reconstruction is based on the methodology presented by Michel et al., (2020) and the corresponding scripts (ClimIndRec version 1.0), which were readapted for a spatial reconstruction. In our study, we focus on the continental area of the European region (34.5°W to 49.5°E and 30.5°N to 74.5°N). The testing and validation period is set from 1900 to 1994 (Figure 2). We use a nesting approach for our study which has the advantage that time series with different temporal coverage can be integrated into the reconstruction. Starting from the longest time frame of reconstruction (i.e., 1600-1994), a new gridded reconstruction is computed as a new $\delta^{18}\text{O}$ timeseries becomes available (see Table 1). At the end of the calculations, the reconstructed datasets
 170 are aggregated to obtain the final reconstruction (Michel et al., 2020). In addition to the reconstruction, validation parameters are calculated for each run of the RF reconstruction using the Coefficient of Efficiency metric (S_{CE}); Supplement Section 1; (Nash and Sutcliffe, 1970).

In order to test the feasibility of our VPD reconstruction, in the final step of the analysis we compare the regional averages and running averages (30 years) of the reconstructed VPD with temperature (Luterbacher et al., 2004), precipitation (Pauling et



175 al., 2006) and Palmer Drought Severity Index (PDSI) reconstructions (Cook et al., 2015) for the three European regions, as
defined by IPCC Sixth Assessment Report (AR6) (IPCC, 2021a; Iturbide et al., 2020): Northern Europe, Central Europe, and
the Mediterranean region. Furthermore, we show maps of the European summer VPD for selected years with extreme positive
VPD anomalies (1868, 1707, 1835) and extreme negative VPD anomalies (1785, 1742, 1747) to investigate the spatial
variability in concordance with past historical data (Brázdil et al., 2013; Brooks and Glasspoole, 1922; Cook et al., 2015;
180 Glaser, 2008; Ionita et al., 2021; Marusek, 2010; Pauling et al., 2006; Trigo et al., 2009). Prior to this mapping, all VPD grid
cells are centered and standardized (z-transformation) to present z-anomalies for each grid cell.

2.4 VPD computation and further pre-processing

The monthly VPD values were calculated based on the equation presented by Barkhordarian et al., (2019) by using the near-
185 surface air temperature (e.g., 2m above the ground) (T) and the dew point temperature (T_d), both in °C. Since dew point
temperature is not available for each grid point of the datasets, we have used T and relative humidity (RH, %) to compute T_d
as follows:

$$T_d = \frac{a_1 * \left(\ln \left(\frac{RH}{100} \right) + \frac{a_2 * T}{a_1 + T} \right)}{a_2 - \left(\ln \left(\frac{RH}{100} \right) + \frac{a_2 * T}{a_1 + T} \right)} \quad (1)$$

Where a_1 and a_2 are defined as $a_1 = 243.04$ and $a_2 = 17.625$. This computation is reliable and is notably used in many climate
190 models (Barkhordarian et al., 2019). We utilize the Clausius–Clapeyron relation, by applying a term for the saturation vapor
content of the air and a term for the actual vapor pressure to calculate VPD as follows in the equation (2) (Barkhordarian et
al., 2019; Behrangi et al., 2016; Marengo et al., 2008; Seager et al., 2015):

$$VPD = c_1 \times e^{\left(\frac{c_2 * T}{c_3 + T} \right)} - c_1 \times e^{\left(\frac{c_2 * T_d}{c_3 + T_d} \right)} \quad (2)$$

195 where $c_1 = 0.611$ kPa, $c_2 = 17.5$, $c_3 = 240.978$ °C, and VPD (kPa) (see WMO (2018) for further information). We compute
seasonal averages DJF (December to February, winter), MAM (March to May, spring), JJA (June to August, summer), and
SON (September to November, fall).

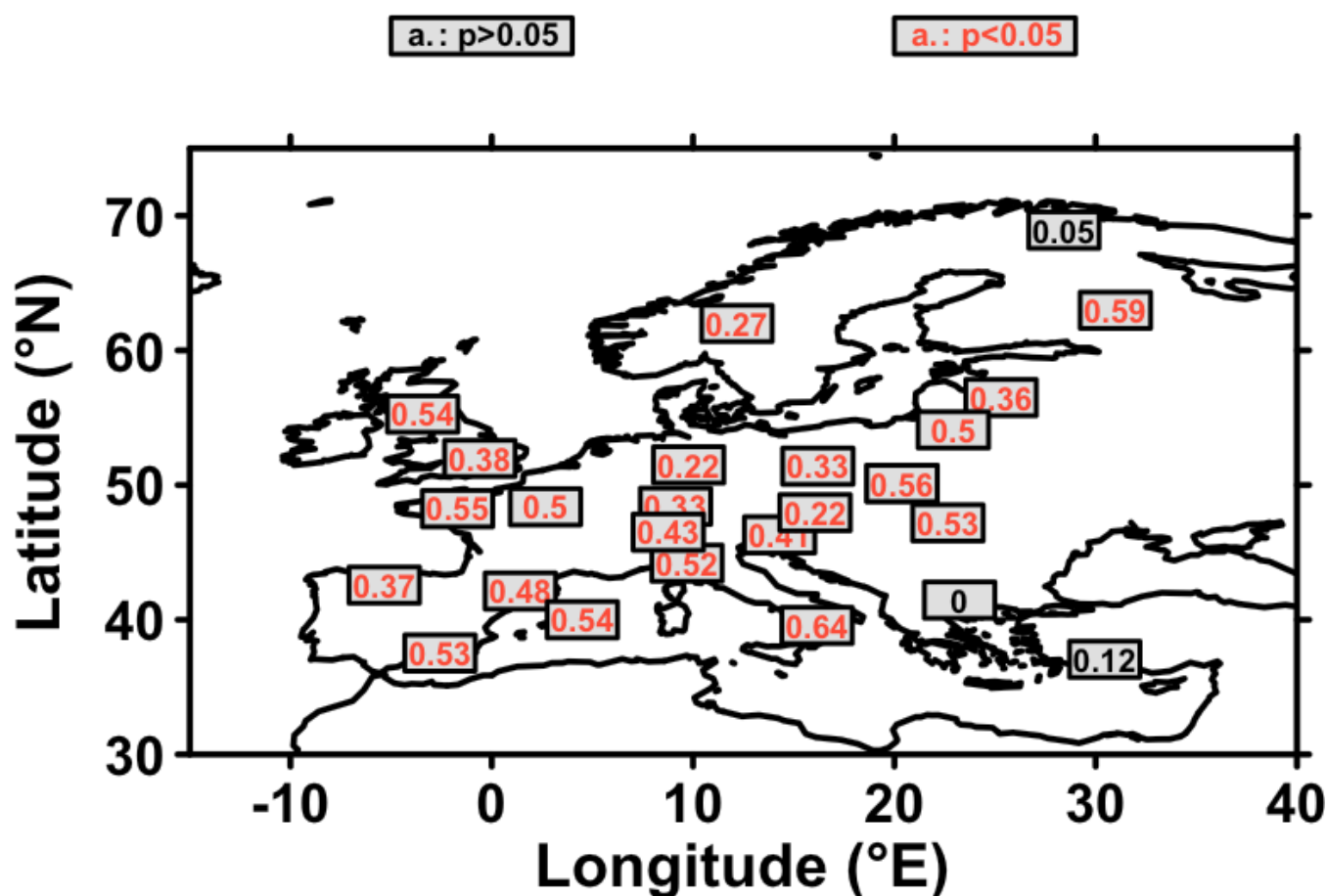
3. Results

200 3.1 Vapor pressure deficit – $\delta^{18}\text{O}$ relationship

The network of $\delta^{18}\text{O}$ time series is significantly correlated with the European Summer VPD over the observational period (i.e.,
1900 – 1994). In Figure 3, we show the correlations of the individual $\delta^{18}\text{O}$ time series with the respective time series of the
grid cell from the calculated VPD of 20CRV3 (Slivinski et al., 2019). High values of significant correlations are reached
between the local summer VPD and the $\delta^{18}\text{O}$ time series (Figure 3). We found that 23 of the 26 sites show significant
205 correlations with local summer VPD at the 95% confidence level, with most of these sites being located in France, Spain,
Germany, Scandinavia, and Great Britain. One time series from Turkey, one from Finland, and one from Bulgaria do not have



a significant correlation with local summer VPD (Figure 3). We note, however, that tree rings from south-eastern Europe (e.g., Turkey, Bulgaria) may be more sensitive to spring VPD rather than summer VPD as demonstrated by a former study (Heinrich et al., 2013). In addition, we notice that there is no influence of the tree species used and no influence of the altitude of sampled trees on the correlations found (Figure 3, Table 1, (Balting et al., 2021)). Based on these results and the relationship between $\delta^{18}\text{O}$ and VPD variability depicted above, we can argue that $\delta^{18}\text{O}$ in tree-ring cellulose can be used as a reliable proxy to perform the reconstruction of VPD for the summer months (JJA).



215 **Figure 3: Correlation of the $\delta^{18}\text{O}$ time series with local summer VPD for the period 1900 to 1994.** The significance of correlations is calculated using a Student t-test for correlation with corrected degrees of freedom from time series as in McCarthy et al., (2015) and Michel et al., (2020). Significant correlations at the 95% confidence level are highlighted in red ($p < 0.05$).

220



3.2 Validation statistics

Since we used a nesting approach in our study, we calculated and optimized our reconstruction by using cross validation (Michel et al., 2020). We had 13 RF models in total, each starting from time steps where at least one time series from the tree-ring network becomes available. The quality of the reconstruction has been described with the Nash–Sutcliffe model efficiency coefficient ($S_{\{CE\}}$) (Supplement Section 1), which is shown in Figure 4 for four selected time steps (1600 – 1699, 1700 – 1799, 1800 – 1899, and 1900 – 1999). Using $S_{\{CE\}}$ scores, the gridded reconstruction is not filled when they are significantly negative at the 95% confidence level. When $S_{\{CE\}}$ scores < 0 , it means that a simple sample average over the testing period is better than the output given by our statistical model. Contrarily, $S_{\{CE\}}$ scores > 0 means that the statistical model gives a more reliable reconstruction than the average over the testing sample, the associated reconstruction is thereby considered reliable in this study.

For the first time step 1600 - 1699, $S_{\{CE\}}$ scores indicate a satisfactory quality (i.e., positive $S_{\{CE\}}$ scores at the 95% confidence level) for the reconstruction of VPD for Northeast Spain, Italy, Greece, France, Germany, and large parts of Scandinavia (Figure 4a). These regions coincide with the locations of the eleven available time series for this time step.

235

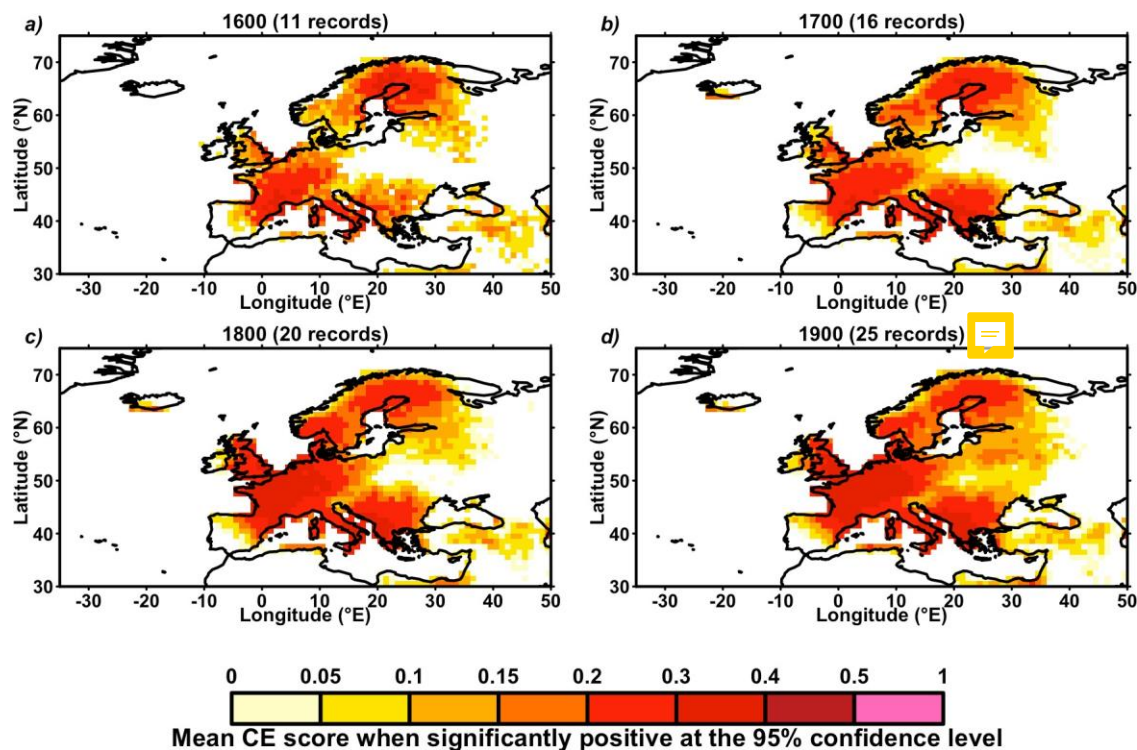


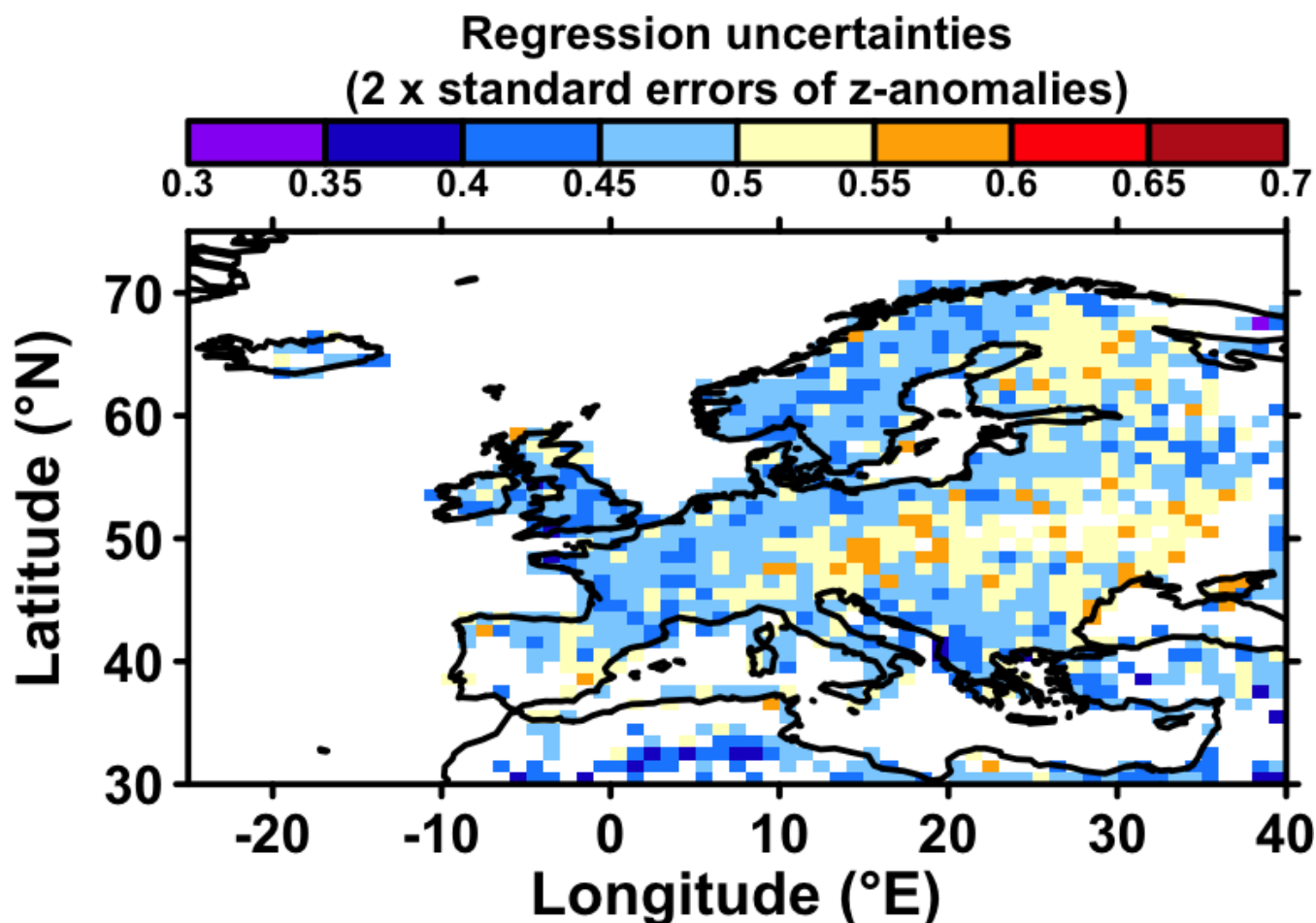
Figure 4: The Nash–Sutcliffe $S_{\{CE\}}$ for four different time slices. The colored areas show the regions where the model set up has a suitable quality, which was tested with a one-sided Student's t-test, on the $S_{\{CE\}}$ scores obtained for testing samples ($p < 0.05$). The significance of correlations is calculated as in McCarthy et al., (2015) and Michel et al., (2020).



240

According to validation scores, our reconstruction is robust over large parts of Europe since 1600 (Figure 4a). From 1700 onwards, when our $\delta^{18}\text{O}$ network has increased to 16 time series, the validation scores became higher and the spatial coverage of grid points with a significantly robust reconstruction at the 95% confidence level now expands to some parts of Eastern Europe and the whole Scandinavian region (Figure 4b). A further improvement of the $S_{\{CE\}}$ values can be observed for the time span 1800 - 1899 (Figure 4c), whereby the most noticeable feature is that Great Britain is now largely covered by grid points with a significantly robust reconstruction at the 95% confidence level. This improvement is due to the fact that another time series from Scotland has been included in the analysis, for this time slice. Finally, for the last time step (i.e., 1901 – 1994), for which all 26 $\delta^{18}\text{O}$ time series are now available, an improvement in the spatial coverage of the reconstruction is found, in particular, a large gap in Eastern Europe is now robustly covered by our reconstruction, due to an additional time series from Romania, which became available from 1900 onwards (Figure 4d). It can also be noted that adjacent regions of Europe, such as parts of Turkey also have a suitable quality for reconstructing past VPD variability changes since a tree-ring series is available in this region. The overall spatial strength of the network is in Southern, Western, and Northern Europe, whereas Eastern Europe can only be partially covered. Therefore, only those grid cells with a satisfactory reconstruction performance (where the mean $S_{\{CE\}}$ scores are significantly positive at the 95% confidence level) will be included in the following analyses.

In addition to the validation scores, we also computed and provided regression uncertainties (Figure 5) in order to evaluate where and when the reconstruction is reliable. For this, the standard errors were first calculated as the average of squared distance between observations and the reconstructed time series over the historical period (1900-1994). The uncertainties for each reconstructed time series from the grid cells (Figure 5) are then defined as an envelope of two times the regression standard errors above and below the reconstructed time series. Overall, the validation statistics passed the conventional verification tests, and the obtained statistical test results indicate that the reconstruction model was statistically sound and can be used for the reconstruction of summer VPD values at the European scale.



265 **Figure 5: Regression uncertainties for each grid cell.** Uncertainties are calculated as two times the regression standard errors of VPD z-anomalies.

3.3 Temporal variability of the European summer VPD reconstruction

270 The VPD reconstruction for the Mediterranean region shows the largest VPD values and higher variability compared to the other two regions (Figure 6a, b). It is noticeable that at the beginning of the reconstruction period (1610-1650), the VPD values decrease ($\beta = -0.0017 \text{ kPa}\cdot\text{year}^{-1}$; $0.05 < p\text{-value} < 0.01$), which is followed by a VPD increase leading to an almost constant VPD level during the Late Maunder Minimum (~1715). From the end of the Maunder Minimum, the VPD decreased steadily until 1761, where it remained at a similar level until 1773. This is followed by a short increase, which is stopped at the beginning of the Dalton Minimum and leads to a decreasing VPD. The minimum of VPD value is also reached during this period (VPD=0.96 kPa for the year 1814). After the Dalton Minimum (~1830), the VPD rises again ($\beta = 0.0003 \text{ kPa}\cdot\text{year}^{-1}$; $0.05 < p\text{-value} < 0.01$). Furthermore, the reconstructed VPD time series shows similar variations as for Central Europe, but most pronounced in the last 150 years. Low periods of variability are shown for example between the end of the 19th century and



the beginning of the 20th century as well as for the 1960s and 70s. In total, the three years with the lowest VPD z-anomalies in this region are 1735, 1814, and 1876 whereas the years with the highest VPD are 1682, 1686, and 1945.

280 The VPD reconstruction for Central Europe (Figure 6c,d) shows that VPD increases from 1600 up to the Late Maunder Minimum (i.e., the early 1700s) ($m = 0.0007 \text{ kPa}\cdot\text{year}^{-1}$; p-value < 0.01 , where m is the linear regression slope). The maximum of the 30-year rolling time series is reached in 1697 (VPD = 0.6398 kPa $> 2.4 \times \sigma$, where σ is the standard deviation of the time series). This increase is followed by a downward trend of VPD in Central Europe which ends in 1743 ($m = -0.0014 \text{ kPa}\cdot\text{year}^{-1}$; $0.01 < \text{p-value} < 0.05$). The period 1740 to 1760 is characterized by very low VPD values and the lowest 30-year

285 rolling VPD. From this time on, the rolling average VPD is characterized by a rising trend ($\beta = 0.0002 \text{ kPa}\cdot\text{year}^{-1}$; p-value < 0.01), but low values are reached during the Dalton Minimum (1790 to 1830). Furthermore, the VPD reconstruction is characterized by a significant 60 to 80 years variability, where the lowest values are reached during the periods 1890 to 1920 and 1960 to 1980 (Figure S2). In total, the three years with the lowest VPD in this region are 1814, 1838, and 1980 whereas the years with the highest VPD are 1687, 1707, and 1835.

290 The average VPD reconstruction for Northern Europe (Figure 6e, f) shows significant differences in variability as well as in the long-term mean. Northern Europe shows the lowest VPD of all three regions, which is due to the comparably low temperatures and high humidity in this area. The increase of VPD between 1620 and 1660 is significant ($m = 0.0017 \text{ kPa}\cdot\text{year}^{-1}$; p-value < 0.01), with the highest VPD value of the 400 years being reached in 1652 (VPD = 0.4619 kPa $> 2.7 \times \sigma$). However, we note that this increase during the Late Maunder Minimum (1675-1715; considered the coldest phase of the Little Ice Age

295 in Europe (Brönnimann, 2015) is not as long-lasting as the former increase from 1620 to 1660. The VPD starts to decrease again from the year 1700. The subsequent drop lasts until the 1720 to 1730 period, after which the time series shows further low-frequency variability and an upward tendency in the 30-year rolling average that lasts until the end of the 20th century ($m = 0.00002 \text{ kPa}\cdot\text{year}^{-1}$; p-value < 0.01). The three years with the lowest VPD in this region are 1632, 1674, and 1802 whereas the years with the highest VPD are 1652, 1959, and 1973.

300

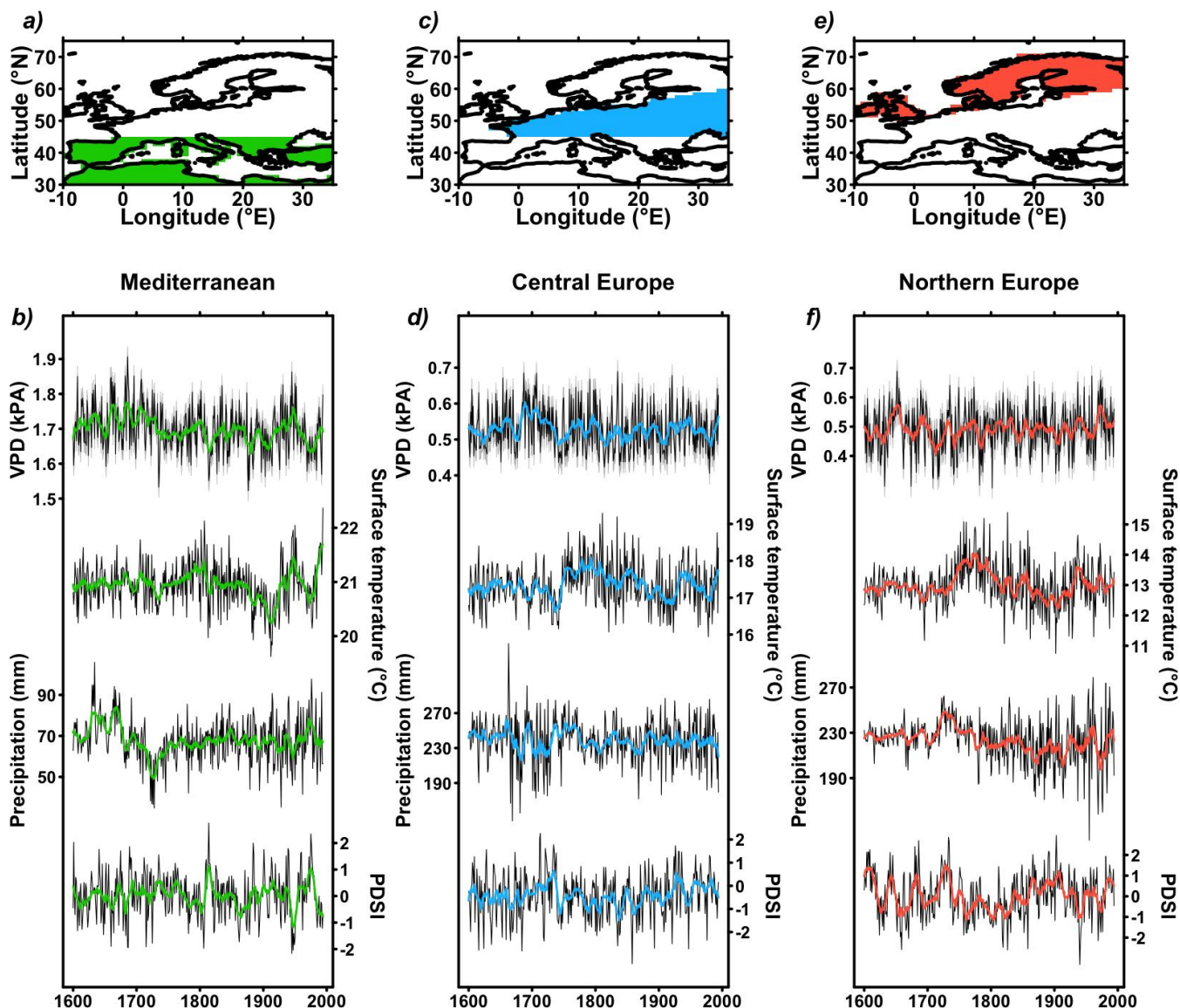
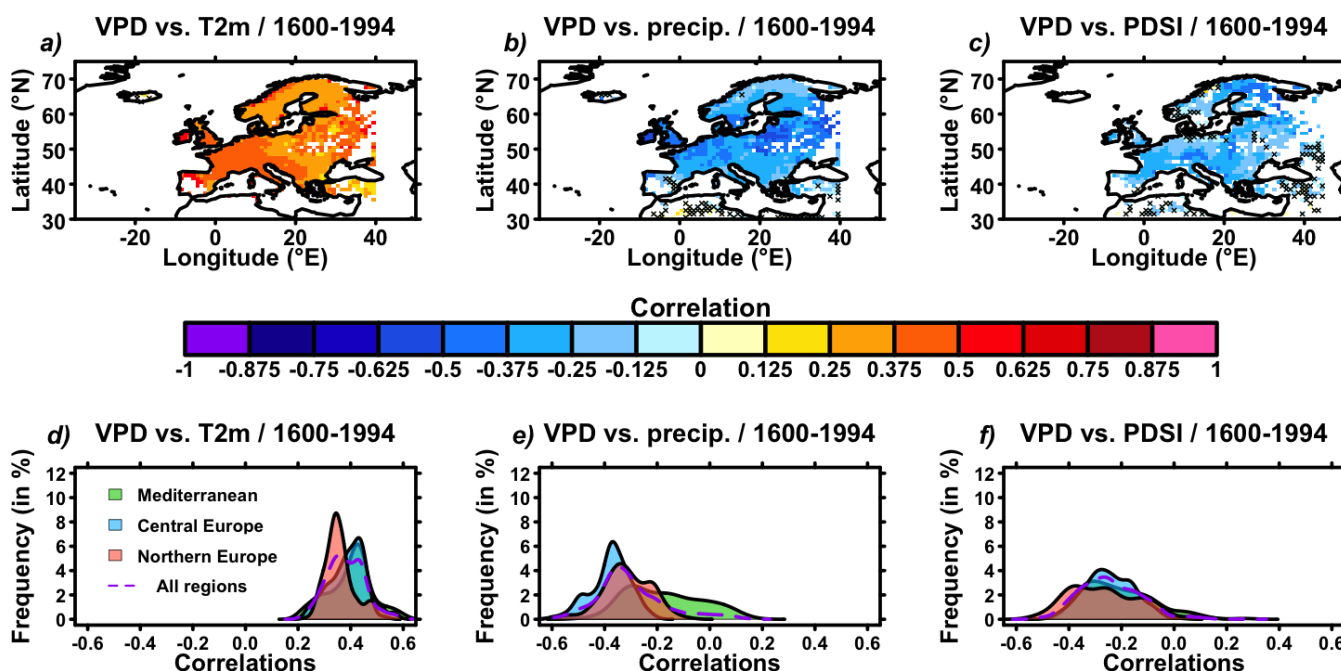


Figure 6: Temporal variability of the VPD reconstruction. Maps (a, c, e) give the location of regions investigated: Mediterranean (a, green), Central Europe (c, blue), and Northern Europe (f, red), following the IPCC AR6 definition (Iturbide et al., 2020). Area-averaged reconstructed time series (b, d, f) for (top to bottom): VPD (this study), surface temperature (Luterbacher et al., 2004), precipitation (Pauling et al., 2006), and PDSI (Cook et al., 2015) for the period 1600-1994, for the same three regions. For VPD timeseries in b, d, f, grey-shaded areas give the range of spatially averaged uncertainties from Figure 5 at the annual timescale.



3.4 Validation of the VPD reconstruction by comparison with other datasets

In order to test the feasibility of our VPD reconstruction, in the following two sub-sections we compare the spatio-temporal variability of our VPD reconstruction with other datasets available for the same time span. Time series from Figure 6b, d, f show some interesting similarities between our summer VPD reconstruction and former ones based on different climatic variables (e.g., precipitation, temperature, drought indicators) (Cook et al., 2015; Luterbacher et al., 2004; Pauling et al., 2006). For the overlap period of these reconstructions (1600-1994), we find consistent positive correlations with area-averaged reconstructed summer temperatures at 2 meters (T2m, (Luterbacher et al., 2004)). The obtained correlations vary between $r=0.36$ ($p<0.01$) for the Mediterranean region, $r=0.31$ ($p<0.01$) for central Europe, and $r=0.38$ ($p<0.01$) for northern Europe (Figure 7). When averaged over the same three regions, an opposite (negative) relationship is found between our VPD reconstruction and a summer precipitation reconstruction (Pauling et al., 2006), where correlations for spatially averaged time series are: $r=-0.26$ ($p<0.01$) for the Mediterranean regions, $r=-0.35$ ($p<0.01$) for central Europe, and $r=-0.39$ ($p<0.01$) for northern Europe (Figure 7). The same results are found when we use a drought indicator, namely the Palmer Drought Sensitivity Index (PDSI). In the case of PDSI, we find significant negative correlations for the three analysed regions, namely: $r=-0.39$ ($p<0.01$) for the Mediterranean regions, $r=-0.24$ ($p<0.01$) for central Europe, and $r=-0.34$ ($p<0.01$) for northern Europe (Figure 7). Interestingly, the Mediterranean region has highest correlations on average for T2m whereas it has the lowest correlations for precipitation and PDSI.



330 **Figure 7: Comparison with former climate field reconstructions.** a-c Correlations between the VPD reconstruction from this study and other climate reconstructions: a) temperature at two meters (T2m) (Luterbacher et al., 2004); b) precipitation



(precip) (Pauling et al., 2006); and c) Palmer Drought Sensitivity Index (PDSI) (Cook et al., 2015); for the period 1600-1994. Black crosses indicate no significance at the 90% confidence level. (d-f) Distribution of correlations from a-c for the same three variables, respectively, for the three regions investigated: Mediterranean (green), Central Europe (blue), Northern Europe (red), and all regions (purple dashed line), following IPCC AR6 (Iturbide et al., 2020), Figure 5).

The spatial correlations with other (paleo)climate reconstructions (the temperature at 2 meters, T2m (Luterbacher et al., 2004); precipitation (Pauling et al., 2006); and PDSI (Cook et al., 2015) are given in Figure 7a-c. It appears that for all three variables, significant correlations are found, with a focus on western and central Europe, which are the areas with the highest tree-ring data coverage (Figure 1, Table 1) and show the highest $S_{\{CE\}}$ validation scores (Figure 4). Taking into account the size of the spatial extension (the whole of Europe) and the time span (400 years) of the correlated data sets, the modest (lower/higher than ± 0.2), but significant correlation coefficients represent a satisfactory result. Therefore the significant correlations found for most regions highlight the important accordance and consistency between the summer VPD reconstruction and former summer climate reconstructions (Cook et al., 2015; Luterbacher et al., 2004; Pauling et al., 2006).

345

3.5 Comparison of the temporal variability with other reconstructions

In this section, we compare the temporal variability of VPD with existing reconstructions of summer temperature (Luterbacher et al., 2004), precipitation (Pauling et al., 2006), and drought (PDSI) reconstruction (Cook et al., 2015) in Figure 6, 7, and 8. For Northern Europe, the characteristics of VPD until 1700 show little resemblance with the reconstructions of precipitation and temperature (Figure 6 e, f). However, the PDSI indicates dry conditions for the time of the maximum VPD in 1652 (Figure 6d). Furthermore, the decrease of VPD between 1700 and 1730 is shown as a wet period in the drought reconstruction, which could be a possible explanation for these low values. From 1730 to 1800, the observed strong temperature increase is visible in VPD only partly. A possible reason for this could be the concurrent increase in summer precipitation. Since the temperature and precipitation changes in this region have similar trends, it is difficult to detect the characteristics of the two variables in the VPD time series.

350

For Central Europe, the increase of the VPD until 1700 cannot be explained by the temperature or precipitation reconstruction (Figure 6d). The 30-year running means of both time series show diverging trends. Nevertheless, the reconstruction of the PDSI also shows a trend towards drier conditions from 1670 to 1690 (Figure 6d). However, before the end of the 17th century, the data indicates a wetting trend. Afterwards, the periods of high and low temperature and precipitation match well with the corresponding periods of high and low VPD. For example, the decrease in precipitation and temperature between 1730 and 1745 is also present in the VPD time series. From 1800 onward, the VPD follows closely the pattern of temperature (Supplement Figure S2). However, the variability of the VPD time series is also influenced by the precipitation variability. The precipitation shows strong interannual variability from the second half of the 19th century, but the magnitude is weaker than in the VPD or the temperature time series. The temperature, precipitation, and VPD reconstructions show similar patterns, it gets warmer, there is less precipitation, and the VPD increases in summer. The PDSI, on the other hand, shows a wetting


365



trend from 1800 onwards. We suggest that this could be based on the accumulation processes of precipitation in the preceding months which is represented by the PDSI (Alley, 1984). This could compensate for the increasing temperature and the decreasing precipitation in summer.

For the Mediterranean area, the summer of 1884 is an extreme event in the temperature time series, as it shows the second
370 coldest temperatures for this region in the last 400 years (Figure 6b). Furthermore, it is interesting that the precipitation increased during the Dalton Minimum (from 1790 and 1830) in this region and only decreased towards its end (1805-1810), which can also explain the behavior of the VPD during this period. We suggest that the comparable low temperatures and the high precipitation led to the 1884 extreme year in the VPD time series. After the end of the Dalton Minimum (i.e., 1830), the temperature shows an increasing trend and the course of the curves is very similar to the variability already described for the
375 VPD, even though the magnitude differs. Nevertheless, the periods with high and low temperatures are almost identical to the corresponding periods of the VPD time series after the Dalton Minimum. Since the decrease in precipitation is almost linear in the 30-year mean from 1850, we suggest that, comparatively, the variability of temperatures can be clearly observed in the VPD time series. A similar situation is also described by the drought reconstruction for the Mediterranean area (Figure 6b). Thus, the reconstructed PDSI of Cook et al. 2015 shows wetter conditions towards the middle of the 18th century, which is
380 complemented by the low VPD values for this period. Like the VPD and the temperature reconstructions, the PDSI shows drier conditions after the 1770s, intensifying after the onset of the Dalton Minimum (~1790). Furthermore, the year 1814 is also the year with the wettest conditions in the PDSI time series. After the Dalton Minimum, the anti-correlation between temperature/VPD and the PDSI is again evident, so that variability is also visible.

385 3.6 Extreme years in the VPD reconstruction and comparison of past/historical data

To illustrate the spatial variability of our VPD reconstruction and validate further our reconstruction,  in respect to other available reconstructions or documentary evidences, at the European level, we selected some of the most extreme years (i.e., the three driest summers (1868, 1707, and 1835) and three wettest summers (1785, 1742, and 1747) when considering time frames with significantly positive S_{CE} scores at the 95% confidence level for each grid point (Figure 4), and look at their
390 spatial variability (Figure 8). Since VPD variability and mean state differ strongly for different latitudes, these six extreme years were selected using spatially-averaged normalized VPD values (i.e., z-anomalies). The year 1742 and 1747 are part of a relatively wet period which correspond to strongly decreasing PDSI (Cook et al., 2015; Ionita et al., 2021) for Europe on average, notably for northernmost regions (Figure 6f) as also suggested by Figure 8e,f. Contrarily, the summer of 1835 is characterized by positive anomalies over south, western, and central Europe, with the highest VPD anomalies over France, which is in concordance with the extremely hot summer condition in France during that summer (Marusek, 2010). During the
395 summer of 1835, in Paris, France was recorded 41 hot days and 11 very hot days (Marusek, 2010). Heat and dryness conditions were also registered in Belgium, England, and Switzerland in 1835 (Marusek, 2010), which is in concordance with our results (Figure 8c). Summer 1868 is characterized by positive anomalies over the western, central-eastern, and northern parts of



Europe (Figure 6a). Documentary data indicate a hot and dry summer in England (e.g. on 21 July 1835 in London was recorded
400 a temperature of 34.1°C) (Marusek, 2010).

The year 1785 is the year with the lowest VPD z-anomalies, on average, for all regions (averaged VPD z-anomalies = -0.68
over all Europe) (Figure 8d). Interestingly, this year follows the Laki (Iceland) eruption (Volcano World, 2023) which,
therefore, had significant impacts in terms of increased precipitation and decreased temperatures and favorizing drought
conditions overall (Figure 5). Summer 1785 is characterized by negative anomalies over Europe (Figure 8d). During this
405 summer, thousands of houses were destroyed in Germany by inundations (Marusek, 2010). Also, numerous storms were
registered in England and France, which laid waste to hundreds of villages and farms (Marusek, 2010).

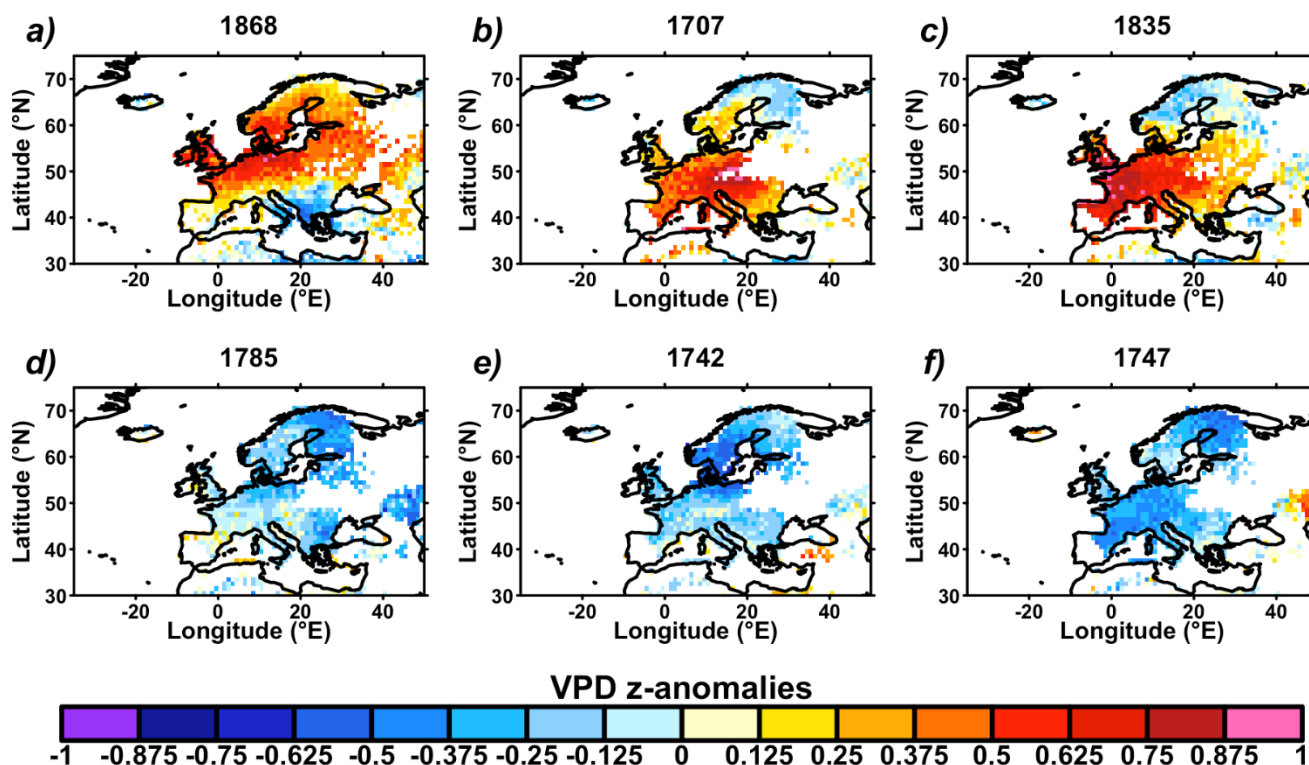


Figure 8: Spatial pattern of VPD anomalies for selected years. Values of each grid cell are VPD z-anomalies (standardized and centered). With respect to the whole period of study (1600-1994). Years were selected as the three with the highest VPD
410 z-anomalies (a-c, a is the highest) and the three with lowest VPD z-anomalies (d-f, d is the lowest) for preindustrial data (1600-1899). Time series only include years where $S_{\{CE\}}$ scores are significantly positive at the 95% confidence level (see Figure 4).

Interestingly, none of the three cases with high VPD anomalies (Figure 8a-c) has overall spatially consistent positive values
415 over the continent compared to low VPD cases (Figure 8d-f). Strong positive anomalies appear over the western and northern



parts of Europe in 1868 (Figure 8a), and western to central Europe in 1707 and 1835 (Figure 8b,c). In all three cases, these large positive anomalies are accompanied by negative anomalies in other regions and form a significant contrast over the continent. Oppositely, the three wettest years happened mainly as a large and spatially consistent set of negative VPD z-anomalies, where only scattered positive values occurred in a few regions (Figure 8d-f).

420

4. Limitations of the reconstruction

The $\delta^{18}\text{O}$ network used in our study (Table 1, Figure 1) is characterized by specific limitations that inevitably influence the quality of the reconstruction presented here. It is likely that the reconstruction may provide some level of sample sites over-representation in Central and Western Europe compared to the ones from Southeast, East, and Northern Europe as shown in Figure 1. These spatial distribution characteristics of sites can also be seen in the validation statistics, where the regions with a good sample density show higher validation scores (Section 3.2). Therefore, further time series from uncovered regions may help in improving the quality and the spatial extent of our reconstruction. Besides the $\delta^{18}\text{O}$ climate signal, the observational/reanalysis data of VPD is given by the ensemble mean of 20CRV3 (Slivinski et al., 2019) for the period 1900 to 1994. Even though the quality and quantity of instrumental data available during this period are comparatively good, the ensemble mean can only represent the variability and diversity of the reanalysis with 80 ensemble members to a limited extent. In our study, the reconstruction is based on the application of the RF algorithm calibrated and evaluated over the period 1900 to 1994. The model is therefore trained to represent exactly this period. Thus, when this model is applied to the previous years, we assume stationarity between the VPD variability and the proxy records, as is generally the case for climate reconstructions (Cook et al., 2015). Since the climate system is not stationary, the assumption of stationarity must be included as a potential source of error. However, the RF approach can represent non-linearities which is not possible with the classical approaches, for example, Principal Component Regression (Cook et al., 2015). Therefore, we compared our reconstruction with other available observational, historical, and proxy based reconstructed data in order to assess errors.

Finally, even if the nested reconstruction approach is used by default for reconstructions (Cook et al., 2007; Freund et al., 2019; Luterbacher et al., 2004; Pauling et al., 2006) to cover the longest possible time range, it is important to check the quality of the model for the respective time range. Therefore, we recommend considering the validation scores for the considered time periods which are also uploaded in the repository.

5. Conclusion & Outlook

Here, we present the first gridded reconstruction of the European summer VPD over the past 400 years, a dataset which was produced to cover a large knowledge gap about past European VPD variability. The obtained results indicate that the past variability of VPD is different for the three regions we investigated, namely: Northern Europe, Central Europe, and the Mediterranean. The lowest VPD values over the past 400 years, as well as the lowest variability, are obtained for Northern Europe. Also, in comparison to the other two regions, Northern Europe is showing the smallest increasing VPD trend in the reconstruction from the mid of the 18th century. The highest VPD values for this region are reached in the mid of the 17th



450 century. Central Europe and the Mediterranean regions reveal stronger trends of increasing VPD (highest VPD on average and highest VPD variability) which can be explained by a precipitation decrease and a temperature increase.

Our results underline that the European VPD values have increased over the last decades. Based on the obtained long-term perspective, we find that this increasing trend in Europe has not started in 2000, but has already begun a few decades after the Late Maunder Minimum with a simultaneous increase of the temperature in the mid-18th century. In the historical context, however, this long-term trend is unique in magnitude and persistence over the last 400 years. Moreover, the results from our study imply that vegetation in Europe has been subject to an increase in VPD for a longer period of time, but that increase has been significantly amplified by recent climate change, especially in Central Europe and the Mediterranean regions. The association between high VPD and a decline in tree growth (Eamus et al., 2013), higher forest mortality (Williams et al., 2013), higher incidence of droughts (Dai, 2013), a decline in crop production (Zhao et al., 2017) and a higher incidence of forest fires (Seager et al., 2015) suggests that high VPD events will become more frequent, with a magnitude that will depend on the amount of greenhouse gas emissions (IPCC, 2021a).

The validation statistics performed to obtain our summer VPD reconstruction, passed all of the conventional verification tests (e.g., Nash–Sutcliffe model efficiency coefficient (S_{CE})), and the obtained statistical test results indicate that the reconstruction model was statistically sound. Thus, we can present, based on this study, the first reconstructions over 400 years of the summer VPD, at the European level. Our spatial reconstruction of summer VPD conditions over Europe, based on tree-ring $\delta^{18}O$ records provides evidence of historical changes and a unique long-term context for recent trends and variability of the summer VPD. Moreover, our VPD reconstruction helps to visualize the local and regional impacts of the current climate change as well as to minimize statistical uncertainties of historical VPD variability, by providing the first gridded reconstruction of the European summer VPD over the past 400 years. Furthermore, the interdisciplinary use of the data should be emphasized, as VPD is a crucial parameter for many climatological processes. As a logical next step, the regional and temporal boundaries of the reconstruction can be extended by using more and longer $\delta^{18}O$ time series from tree-ring cellulose. It is also possible to disentangle the influence of solar events on the VPD on the local, regional, and continental scales.

Contributions

475 D.F.B conceived the ideas and designed the methodology together with S.L.L.M. and V.N. D.F.B analyzed the data, drafted and led the writing of the manuscript with significant inputs from S.L.L.M, M.I., V.N., G.H., M.F., G.H.S., D.N.S., and G.L. All authors contributed critically to the drafts and gave final approval for publication.

Data and Code availability

480 The gridded reconstructed summer VPD over the last 400 years, at the European level, is available here: <https://doi.org/10.5281/zenodo.5958836> (Balting, D. F. et al., 2022). The ISONET oxygen isotope data can be accessed at GFZ Data Services: <https://doi.org/10.5880/GFZ.4.3.2023.001>. The time series of the individual sample sites can be request by the corresponding authors of the mentioned studies in the proxy network Section. The climate data from 20CRv3 is freely



available. The postprocessing of the model and reanalysis output data has been done with the Climate Data Operators
485 (Schulzweida, 2019) and the corresponding Python binding. Furthermore, the reconstruction of the VPD have been done with
a modified version of the ClimIndRec version 1.0 scripts (<https://zenodo.org/record/5716236#.YZkyyi2ZOL8>) in R (version
4.0.2). The required R packages (glmnet, pls, randomForest, ncd4 and dependencies) are freely available.

Competing interests

490 The authors declare that there is no conflict of interest.

Acknowledgment

Funding by the PalEX Project (AWI Strategy Fund) is greatly acknowledged. GL and MI are supported by Helmholtz funding
through the joint program "Changing Earth - Sustaining our Future" (PoF IV) program of the AWI. Funding by the Helmholtz
495 Climate Initiative - REKLIM is gratefully acknowledged. VN was partially supported by a grant of the Ministry of Research,
Innovation and Digitization, CNCS/CCCDI – UEFISCDI, project number PN-III-P1-1.1-PD-2019-0469, within PNCDI III.
All but four tree-ring stable isotope chronologies were established within the project ISONET supported by the European
Union (EVK2-CT-2002-00147 'ISONET'). We want to thank all participants of the ISONET project (L. Andreu, Z. Bednarz,
F. Berninger, T. Boettger, C. M. D'Alessandro, J. Esper, N. Etien, M. Filot, D. Frank, M. Grabner, M. T. Guillemain, E.
500 Gutierrez, M. Haupt, E. Hilarvuori, H. Jungner, M. Kalela-Brundin, M. Krapiec, M. Leuenberger, H.H. Leuschner, N. J.
Loader, V. Masson-Delmotte, A. Pazdur, S. Pawelczyk, M. Pierre, O. Planells, R. Pukiene, C. E. Reynolds-Henne, K. T. Rinne,
Saracino, M. Saurer, E. Sonninen, M. Stievenard, V. R. Switsur, M. Szczepanek, E. Szychowska-Krapiec, L. Todaro, K.
Treydte, J. S. Waterhouse, and M. Weigl). The data from Turkey, Slovenia and Southwest Germany were produced with the
EU-funded project MILLENNIUM (GOCE 017008-2'MILLENNIUM'), special thanks to T. Levanic and R. Touchan. The
505 tree-ring stable isotope chronologies from Bulgaria were established with support of the German Research Foundation DFG
(HE3089-1, GR 1432/11-1) and in cooperation with the administration of Pirin National Park, Bulgaria. Furthermore, we want
to thank Paul Gierz and Christian Stepanek for technical support.

510

515



References

- 520 Ali, M., Prasad, R., Xiang, Y. and Yaseen, Z. M.: Complete ensemble empirical mode decomposition hybridized with random forest and kernel ridge regression model for monthly rainfall forecasts, *J. Hydrol.*, 584, doi:10.1016/j.jhydrol.2020.124647, 2020.
- Alley, W. M.: The Palmer Drought Severity Index: Limitations and Assumptions, *J. Clim.*, 23, 1100–1109 [online] Available from: <http://journal.um-surabaya.ac.id/index.php/JKM/article/view/2203>, 1984.
- 525 Andreu-Hayles, L., Ummenhofer, C. C., Barriendos, M., Schleser, G. H., Helle, G., Leuenberger, M., Gutiérrez, E. and Cook, E. R.: 400 Years of summer hydroclimate from stable isotopes in Iberian trees, *Clim. Dyn.*, 49(1–2), 143–161, doi:10.1007/s00382-016-3332-z, 2017.
- Bair, E. H., Calfa, A. A., Rittger, K. and Dozier, J.: Using machine learning for real-time estimates of snow water equivalent in the watersheds of Afghanistan, *Cryosphere*, 12(5), doi:10.5194/tc-12-1579-2018, 2018.
- 530 Balting, D. F., Ionita, M., Wegmann, M., Helle, G., Schleser, G. H., Rimbu, N., Freund, M. B., Heinrich, I., Caldarescu, D. and Lohmann, G.: Large-scale climate signals of a European oxygen isotope network from tree rings, *Clim. Past*, 17(3), doi:10.5194/cp-17-1005-2021, 2021.
- Barkhordarian, A., Saatchi, S. S., Behrangi, A., Loikith, P. C. and Mechoso, C. R.: A Recent Systematic Increase in Vapor Pressure Deficit over Tropical South America, *Sci. Rep.*, 9(1), doi:10.1038/s41598-019-51857-8, 2019.
- 535 Behrangi, A., Fetzer, E. J. and Granger, S. L.: Early detection of drought onset using near surface temperature and humidity observed from space, *Int. J. Remote Sens.*, 37(16), doi:10.1080/01431161.2016.1204478, 2016.
- Belgiu, M. and Drăgu, L.: Random forest in remote sensing: A review of applications and future directions, *ISPRS J. Photogramm. Remote Sens.*, 114, doi:10.1016/j.isprsjprs.2016.01.011, 2016.
- 540 Boettger, T., Haupt, M., Konller, K., Weise, S. M., Waterhouse, J. S., Rinne, T., Loader, N. J., Sonninen, E., Jungner, H., Masson-Delmotte, V., Stievenard, M., Guillemain, M.-T., Pierre, M., Pazdur, A., Leuenberger, M., Filot, M., Saurer, M., Reynolds, C. E., Helle, G. and Schleser, G. H.: Wood Cellulose Preparation Methods and Mass Spectrometric Analyses of $\delta^{13}\text{C}$, $\delta^{18}\text{O}$, and Nonexchangeable $\delta^2\text{H}$ Values in Cellulose, Sugar, and Starch: An Interlaboratory Comparison, *Anal. Chem.*, 79(12), 4603–4612, doi:10.1021/ac0700023, 2007.
- Brázdil, R., Dobrovolný, P., Trnka, M., Kotyza, O., Řezníčková, L., Valášek, H., Zahradníček, P. and Štěpánek, P.: Droughts in the Czech Lands, 1090–2012 AD, *Clim. Past*, 9(4), doi:10.5194/cp-9-1985-2013, 2013.
- 545 Breiman, L.: Random Forests, *Mach. Learn.*, 45, 5–32, doi:10.1109/ICCECE51280.2021.9342376, 2001.
- Brönnimann, S.: Climatic Changes Since 1700, in *Advances in Global Change Research*, vol. 55., 2015.
- Brooks, C. E. P. and Glasspoole, J.: The drought of 1921 in the British Isles, *Mon. Weather Rev.*, 50(2), 93–93, doi:10.1175/1520-0493(1922)50<93a:tdoitb>2.0.co;2, 1922.
- 550 Churakova Sidorova, O. V., Corona, C., Fonti, M. V., Guillet, S., Saurer, M., Siegwolf, R. T. W., Stoffel, M. and Vaganov, E. A.: Recent atmospheric drying in Siberia is not unprecedented over the last 1,500 years, *Sci. Rep.*, 10(1), doi:10.1038/s41598-020-71656-w, 2020.



- Cook, E. R., Seager, R., Cane, M. A. and Stahle, D. W.: North American drought: Reconstructions, causes, and consequences, *Earth Sci. Rev.*, 81(1), 93–134, doi:10.1016/j.earscirev.2006.12.002, 2007.
- 555 Cook, E. R., Seager, R., Kushnir, Y., Briffa, K. R., Büntgen, U., Frank, D., Krusic, P. J., Tegel, W., van der Schrier, G., Andreu-Hayles, L., Baillie, M., Baittinger, C., Bleicher, N., Bonde, N., Brown, D., Carrer, M., Cooper, R., Čufar, K., Dittmar, C., Esper, J., Griggs, C., Gunnarson, B., Günther, B., Gutierrez, E., Haneca, K., Helama, S., Herzig, F., Heussner, K.-U. U., Hofmann, J., Janda, P., Kontic, R., Köse, N., Kyncl, T., Levanič, T., Linderholm, H., Manning, S., Melvin, T. M., Miles, D., Neuwirth, B., Nicolussi, K., Nola, P., Panayotov, M., Popa, I., Rothe, A., Seftigen, K., Seim, A., Svarva, H., Svoboda, M., Thun, T., Timonen, M., Touchan, R., Trotsiuk, V., Trouet, V., Walder, F., Ważny, T.,
- 560 Wilson, R., Zang, C., Schrier, G. V. Der, Andreu-Hayles, L., Baillie, M., Baittinger, C., Bleicher, N., Bonde, N., Brown, D., Carrer, M., Cooper, R., Eufar, K., Dittmar, C., Esper, J., Griggs, C., Gunnarson, B., Günther, B., Gutierrez, E., Haneca, K., Helama, S., Herzig, F., Heussner, K.-U. U., Hofmann, J., Janda, P., Kontic, R., Köse, N., Kyncl, T., Levaniè, T., Linderholm, H., Manning, S., Melvin, T. M., Miles, D., Neuwirth, B., Nicolussi, K., Nola, P., Panayotov, M., Popa, I., Rothe, A., Seftigen, K., Seim, A., Svarva, H., Svoboda, M., Thun, T., Timonen, M., et al.: Old World megadroughts and pluvials during the Common Era, *Sci. Adv.*, e1500561 6(10), 1–10, doi:10.1126/sciadv.1500561, 2015.
- 565
- Craig, H.: Isotopic standards for carbon and oxygen and correction factors for mass-spectrometric analysis of carbon dioxide, *Geochim. Cosmochim. Acta*, 12(1–2), doi:10.1016/0016-7037(57)90024-8, 1957.
- Dai, A.: Increasing drought under global warming in observations and models, *Nat. Clim. Chang.*, 3(1), 52–58, doi:10.1038/nclimate1633, 2013.
- 570
- Davies, D. and Loader, N. J.: An evaluation of english oak earlywood vessel area as a climate proxy in the UK, *Dendrochronologia*, 64, doi:10.1016/j.dendro.2020.125777, 2020.
- Delcroix, T., Michel, S. L. L., Swingedouw, D., Malaizé, B., Daniau, A.-L., Abarca-del-Rio, R., Caley, T. and Sémah, A.-M.: Clarifying the role of ENSO on Easter Island precipitation changes: Potential environmental implications for the last millennium. XX, XX-XX (202X), *Paleoceanography and Paleoclimatology*, under revi, 2022.
- 575
- Eamus, D., Boulain, N., Cleverly, J. and Breshears, D. D.: Global change-type drought-induced tree mortality: vapor pressure deficit is more important than temperature per se in causing decline in tree health, *Ecol. Evol.*, 3(8), 2711–2729, 2013.
- Etien, N., Daux, V., Masson-Delmotte, V., Stievenard, M., Bernard, V., Durost, S., Guillemin, M. T., Mestre, O. and Pierre, M.: A bi-proxy reconstruction of Fontainebleau (France) growing season temperature from A.D. 1596 to 2000, *Clim. Past*, 4(2), doi:10.5194/cp-4-91-2008, 2008.
- 580
- Ferrio, J. P. and Voltas, J.: Carbon and oxygen isotope ratios in wood constituents of *Pinus halepensis* as indicators of precipitation, temperature and vapour pressure deficit, *Tellus, Ser. B Chem. Phys. Meteorol.*, 57(2), doi:10.1111/j.1600-0889.2005.00137.x, 2005.
- Fletcher, A. L., Sinclair, T. R. and Allen, L. H.: Transpiration responses to vapor pressure deficit in well watered “slow-wilting” and commercial soybean, *Environ. Exp. Bot.*, 61(2), doi:10.1016/j.envexpbot.2007.05.004, 2007.
- 585



- Freund, M. B., Henley, B. J., Karoly, D. J., McGregor, H. V., Abram, N. J. and Dommenges, D.: Higher frequency of Central Pacific El Niño events in recent decades relative to past centuries, *Nat. Geosci.*, 12(6), doi:10.1038/s41561-019-0353-3, 2019.
- Fritts, H. C.: *Tree Rings and Climate*, Academic Press, London., 1976.
- 590 Gagen, M., Battipaglia, G., Daux, V., Duffy, J., Dorado-Liñán, I., Hayles, L. A., Martínez-Sancho, E., McCarroll, D., Shestakova, T. A. and Treydte, K.: Climate Signals in Stable Isotope Tree-Ring Records BT - Stable Isotopes in Tree Rings: Inferring Physiological, Climatic and Environmental Responses, in *Stable Isotopes in Tree Rings. Tree Physiology*, edited by R. T. W. Siegwolf, J. R. Brooks, J. Roden, and M. Saurer, pp. 537–579, Springer International Publishing, Cham., 2022.
- 595 Glaser, R.: *Klimageschichte Mitteleuropas: 1200 Jahre Wetter, Klima, Katastrophen*, Primus Verlag, Darmstadt., 2008.
- González-González, B. D., Vázquez-Ruiz, R. A. and García-González, I.: Effects of climate on earlywood vessel formation of *quercus robur* and *q. Pyrenaica* at a site in the northwestern iberian peninsula, *Can. J. For. Res.*, 45(6), doi:10.1139/cjfr-2014-0436, 2015.
- Good, S. P., Noone, D. and Bowen, G.: Hydrologic connectivity constrains partitioning of global terrestrial water fluxes, *Science* (80-.), 349(6244), doi:10.1126/science.aaa5931, 2015.
- 600 Grossiord, C., Buckley, T. N., Cernusak, L. A., Novick, K. A., Poulter, B., Siegwolf, R. T. W., Sperry, J. S. and McDowell, N. G.: Plant responses to rising vapor pressure deficit, *New Phytol.*, 226(6), doi:10.1111/nph.16485, 2020.
- Hafner, P., McCarroll, D., Robertson, I., Loader, N. J., Gagen, M., Young, G. H. F., Bale, R. J., Sonninen, E. and Levanič, T.: A 520 year record of summer sunshine for the eastern European Alps based on stable carbon isotopes in larch tree rings, *Clim. Dyn.*, 43(3), 971–980, doi:10.1007/s00382-013-1864-z, 2014.
- 605 Haupt, M., Weigl, M., Grabner, M. and Boettger, T.: A 400-year reconstruction of July relative air humidity for the Vienna region (eastern Austria) based on carbon and oxygen stable isotope ratios in tree-ring latewood cellulose of oaks (*Quercus petraea* Matt. Liebl.), *Clim. Change*, 105(1), 243–262, doi:10.1007/s10584-010-9862-1, 2011.
- Heinrich, I., Touchan, R., Dorado Liñán, I., Vos, H. and Helle, G.: Winter-to-spring temperature dynamics in Turkey derived from tree rings since AD 1125, *Clim. Dyn.*, 41(7–8), doi:10.1007/s00382-013-1702-3, 2013.
- 610 Helama, S., Läänelaid, A., Raisio, J., Mäkelä, H. M., Hilasvuori, E., Jungner, H. and Sonninen, E.: Oak decline analyzed using intraannual radial growth indices, $\delta^{13}\text{C}$ series and climate data from a rural hemiboreal landscape in southwesternmost Finland, *Environ. Monit. Assess.*, 186(8), doi:10.1007/s10661-014-3731-8, 2014.
- Hilasvuori, E., Berninger, F., Sonninen, E., Tuomenvirta, H. and Jungner, H.: Stability of climate signal in carbon and oxygen isotope records and ring width from Scots pine (*Pinus sylvestris* L.) in Finland, *J. Quat. Sci.*, 24(5), doi:10.1002/jqs.1260, 2009.
- 615 Ionita, M., Dima, M., Nagavciuc, V., Scholz, P. and Lohmann, G.: Past megadroughts in central Europe were longer, more severe and less warm than modern droughts, *Commun. Earth Environ.*, 2(1), 61, doi:10.1038/s43247-021-00130-w, 2021.



- 620 IPCC: Climate Change 2021: The Physical Science Basis. Contribution of Working Group I to the Sixth Assessment Report of the Intergovernmental Panel on Climate Change, edited by V. Masson-Delmotte, P. Zhai, A. Pirani, S. L. Connors, C. Péan, S. Berger, N. Caud, Y. Chen, L. Goldfarb, M. I. Gomis, M. Huang, K. Leitzell, E. Lonnoy, J. B. R. Matthews, T. K. Maycock, T. Waterfield, O. Yelekçi, R. Yu, and B. Zhou, Cambridge University Press. In Press., 2021a.
- IPCC: Summary for policymakers, in Climate Change 2021: The Physical Science Basis. Contribution of Working Group I to the Sixth Assessment Report of the Intergovernmental Panel on Climate Change, edited by V. Masson-Delmotte, P. Zhai, A. Pirani, S. L. Connors, C. Péan, S. Berger, N. Caud, Y. Chen, L. Goldfarb, M. I. Gomis, M. Huang, K. Leitzell, E. Lonnoy, J. B. R. Matthews, T. K. Maycock, T. Waterfield, O. Yelekçi, R. Yu, and B. Zhou, pp. 3–22, Cambridge University Press, Cambridge, United Kingdom and New York, NY, USA., 2021b.
- 625
- ISONET Project Members, Schleser, G. H., Andreu-Hayles, L., Bednarsz, Z., Berninger, F., Boettger, T., Dorado-Liñán, I., Esper, J., Grabner, M., Gutiérrez, E., Helle, G., Hilasvuori, E., Jugner, H., Kalela-Brundin, M., Krąpiec, M., Leuenberger, M., Loader, N. J., Masson-Delmotte, V., Pawełczyk, S., Pazdur, A., Pukienė, R., Rinne-Garmston, K. T., Saracino, A., Saurer, M., Sonninen, E., Stiévenard, M., Switsur, V. R. Szychowska-Krąpiec, E. Szczepanek, M., Todaro, L., Treydte, K., Vitas, A., Waterhouse, J. S., Weigl-Kuska, M. and Wimmer, R.: Stable oxygen isotope ratios of tree-ring cellulose from the site network of the EU-Project “ISONET,” GFZ Data Serv., doi:https://doi.org/10.5880/GFZ.4.3.2023.001, 2023.
- 630
- Iturbide, M., Gutiérrez, J. M., Alves, L. M., Bedia, J., Cerezo-Mota, R., Gimeno-Caballero, E., Cofiño, A. S., Luca, A. Di, Faria, S. H., Gorodetskaya, I. V., Hauser, M., Herrera, S., Hennessy, K., Hewitt, H. T., Jones, R. G., Krakovska, S., Manzanar, R., Martínez-Castro, D., Narisma, G. T., Nurhati, I. S., Pinto, I., Seneviratne, S. I., Hurk, B. van den and Vera, C. S.: An update of IPCC climate reference regions for subcontinental analysis of climate model data: definition and aggregated datasets, *Earth Syst. Sci. Data*, 12(4), doi:10.5194/essd-12-2959-2020, 2020.
- 640
- Jasechko, S., Sharp, Z. D., Gibson, J. J., Birks, S. J., Yi, Y. and Fawcett, P. J.: Terrestrial water fluxes dominated by transpiration, *Nature*, 496(7445), doi:10.1038/nature11983, 2013.
- Josse, J. and Husson, F.: missMDA: A Package for Handling Missing Values in Multivariate Data Analysis, *J. Stat. Softw.*, 70(1 SE-Articles), 1–31, doi:10.18637/jss.v070.i01, 2016.
- 645
- Kahmen, A., Sachse, D., Arndt, S. K., Tu, K. P., Farrington, H., Vitousek, P. M. and Dawson, T. E.: Cellulose $\delta^{18}\text{O}$ is an index of leaf-to-air vapor pressure difference (VPD) in tropical plants, *Proc. Natl. Acad. Sci. U. S. A.*, 108(5), doi:10.1073/pnas.1018906108, 2011.
- Labuhn, I., Daux, V., Pierre, M., Stievenard, M., Girardclos, O., Féron, A., Genty, D. and Masson-Delmotte, V., Mestre, O.: Tree age, site and climate controls on tree ring cellulose $\delta^{18}\text{O}$: A case study on oak trees from south-western France, *Dendrochronologia*, 32, 78–89, doi:doi:10.1016/j.dendro.2013.11.001, 2014.
- 650
- Labuhn, I., Daux, V., Girardclos, O., Stievenard, M., Pierre, M. and Masson-Delmotte, V.: French summer droughts since 1326 CE: A reconstruction based on tree ring cellulose $\delta^{18}\text{O}$, *Clim. Past*, 12(5), 1101–1117, doi:doi:10.5194/cp-12-1101-2016, 2016.



- Lawrence, M. G.: The relationship between relative humidity and the dewpoint temperature in moist air: A simple conversion
655 and applications, *Bull. Am. Meteorol. Soc.*, 86(2), doi:10.1175/BAMS-86-2-225, 2005.
- Leonelli, G., Coppola, A., Salvatore, M. C., Baroni, C., Battipaglia, G., Gentilesca, T., Ripullone, F., Borghetti, M., Conte, E.
and Tognetti, R.: Climate signals in a multispecies tree-ring network from central and southern Italy and reconstruction
of the late summer temperatures since the early 1700s, *Clim. Past*, 13, 1451–1471, 2017.
- Li, J., Wang, Z., Lai, C. and Zhang, Z.: Tree-ring-width based streamflow reconstruction based on the random forest algorithm
660 for the source region of the Yangtze River, China, *Catena*, 183, doi:10.1016/j.catena.2019.104216, 2019.
- Lindgren, A., Lu, Z., Zhang, Q. and Hugelius, G.: Reconstructing Past Global Vegetation With Random Forest Machine
Learning, Sacrificing the Dynamic Response for Robust Results, *J. Adv. Model. Earth Syst.*, 13(2),
doi:10.1029/2020MS002200, 2021.
- Liu, X., Zhang, X., Zhao, L., Xu, G., Wang, L., Sun, W., Zhang, Q., Wang, W., Zeng, X. and Wu, G.: Tree ring 180 reveals
665 no long-term change of atmospheric water demand since 1800 in the northern Great Hinggan Mountains, China, *J.
Geophys. Res. Atmos.*, 122, 6697–6712, 2017.
- Luterbacher, J., Dietrich, D., Xoplaki, E., Grosjean, M. and Wanner, H.: European Seasonal and Annual Temperature
Variability, Trends, and Extremes since 1500, *Science (80-.)*, 303(5663), 1499–1503, doi:10.1126/science.1093877,
2004.
- 670 Marengo, J. A., Nobre, C. A., Tomasella, J., Oyama, M. D., de Oliveira, G. S., de Oliveira, R., Camargo, H., Alves, L. M. and
Brown, I. F.: The drought of Amazonia in 2005, *J. Clim.*, 21(3), doi:10.1175/2007JCLI1600.1, 2008.
- Marusek, J. A.: A Chronological Listing of Early Weather Events, *breadandbutter-science*, 580, 2010.
- Maxwell, A. E., Warner, T. A. and Fang, F.: Implementation of machine-learning classification in remote sensing: An applied
review, *Int. J. Remote Sens.*, 39(9), doi:10.1080/01431161.2018.1433343, 2018.
- 675 McCarroll, D. and Loader, N. J.: Stable isotopes in tree rings, *Quat. Sci. Rev.*, 23(7–8), 771–801,
doi:http://dx.doi.org/10.1016/j.quascirev.2003.06.017, 2004.
- McCarthy, G. D., Haigh, I. D., Hirschi, J. J.-M., Grist, J. P. and Smeed, D. A.: Ocean impact on decadal Atlantic climate
variability revealed by sea-level observations, *Nature*, 521(7553), 508–510, doi:10.1038/nature14491, 2015.
- Michel, S., Swingedouw, D., Chavent, M., Ortega, P., Mignot, J. and Khodri, M.: Reconstructing climatic modes of variability
680 from proxy records using ClimIndRec version 1.0, *Geosci. Model Dev.*, 13(2), doi:10.5194/gmd-13-841-2020, 2020.
- Michel, S. L. L., Swingedouw, D., Ortega, P., Gastineau, G., Mignot, J., McCarthy, G. and Khodri, M.: Early warning signal
for a tipping point suggested by a millennial Atlantic Multidecadal Variability reconstruction, *Nat. Commun.*, 13(1),
5176, doi:10.1038/s41467-022-32704-3, 2022.
- Mohr, C. H., Manga, M., Helle, G., Heinrich, I., Giese, L. and Korup, O.: Trees Talk Tremor Wood Anatomy and Content
685 Reveal Contrasting Tree-Growth Responses to Earthquakes, *J. Geophys. Res. Biogeosciences*, 126, e2021JG006385,
doi:https://doi.org/10.1029/2021JG006385, 2021.
- Nagavciuc, V., Ionita, M., Perşoiu, A., Popa, I., Loader, N. J. and McCarroll, D.: Stable oxygen isotopes in Romanian oak tree



- rings record summer droughts and associated large-scale circulation patterns over Europe, *Clim. Dyn.*, 52, 6557–6568, doi:doi.org/10.1007/s00382-018-4530-7, 2019.
- 690 Nagavciuc, V., Ionita, M., Kern, Z., McCarroll, D. and Popa, I.: A ~700 years perspective on the 21st century drying in the eastern part of Europe based on $\delta^{18}\text{O}$ in tree ring cellulose, *Commun. Earth Environ.*, 3, 277, doi:10.1038/s43247-022-00605-4, 2022.
- Nash, J. E. and Sutcliffe, J. V.: River flow forecasting through conceptual models part I - A discussion of principles, *J. Hydrol.*, 10(3), 282–290, doi:10.1016/0022-1694(70)90255-6, 1970.
- 695 Novick, K. A., Ficklin, D. L., Stoy, P. C., Williams, C. A., Bohrer, G., Oishi, A. C., Papuga, S. A., Blanken, P. D., Noormets, A., Sulman, B. N., Scott, R. L., Wang, L. and Phillips, R. P.: The increasing importance of atmospheric demand for ecosystem water and carbon fluxes, *Nat. Clim. Chang.*, 6(11), doi:10.1038/nclimate3114, 2016.
- Pauling, A., Luterbacher, J., Casty, C. and Wanner, H.: Five hundred years of gridded high-resolution precipitation reconstructions over Europe and the connection to large-scale circulation, *Clim. Dyn.*, 26(4), 387–405, doi:10.1007/s00382-005-0090-8, 2006.
- 700 Prasad, R., Ali, M., Kwan, P. and Khan, H.: Designing a multi-stage multivariate empirical mode decomposition coupled with ant colony optimization and random forest model to forecast monthly solar radiation, *Appl. Energy*, 236, doi:10.1016/j.apenergy.2018.12.034, 2019.
- Qu, Y., Zhu, Z., Chai, L., Liu, S., Montzka, C., Liu, J., Yang, X., Lu, Z., Jin, R., Li, X., Guo, Z. and Zheng, J.: Rebuilding a microwave soil moisture product using random forest adopting amsr-e/amsr2 brightness temperature and smap over the Qinghai–Tibet Plateau, China, *Remote Sens.*, 11(6), doi:10.3390/rs11060683, 2019.
- 705 Reichstein, M., Camps-Valls, G., Stevens, B., Jung, M., Denzler, J., Carvalhais, N. and Prabhat: Deep learning and process understanding for data-driven Earth system science, *Nature*, 566(7743), doi:10.1038/s41586-019-0912-1, 2019.
- Restaino, C. M., Peterson, D. L. and Littell, J.: Increased water deficit decreases Douglas fir growth throughout western US forests, *Proc. Natl. Acad. Sci. U. S. A.*, 113(34), doi:10.1073/pnas.1602384113, 2016.
- 710 Rinne, K. T., Loader, N. J., Switsur, V. R. and Waterhouse, J. S.: 400-year May - August precipitation reconstruction for Southern England using oxygen isotopes in tree rings, *Quat. Sci. Rev.*, 60, 13–25, doi:10.1016/j.quascirev.2012.10.048, 2013.
- Rodriguez-Galiano, V. F., Ghimire, B., Rogan, J., Chica-Olmo, M. and Rigol-Sanchez, J. P.: An assessment of the effectiveness of a random forest classifier for land-cover classification, *ISPRS J. Photogramm. Remote Sens.*, 67(1), doi:10.1016/j.isprsjprs.2011.11.002, 2012.
- 715 Roibu, C. C., Palaghianu, C., Nagavciuc, V., Ionita, M., Sfecla, V., Mursa, A., Crivellaro, A., Stirbu, M. I., Cotos, M. G., Popa, A., Sfecla, I. and Popa, I.: The Response of Beech (*Fagus sylvatica* L.) Populations to Climate in the Easternmost Sites of Its European Distribution, *Plants*, 11(23), doi:10.3390/plants1123310, 2022.
- 720 Running, S. W.: Environmental control of leaf water conductance in conifers, *Can. J. For. Res.*, 6(1), doi:10.1139/x76-013, 1976.



- Saurer, M., Cherubini, P., Reynolds-Henne, C. E., Treydte, K. S., Anderson, W. T. and Siegwolf, R. T. W.: An investigation of the common signal in tree ring stable isotope chronologies at temperate sites, *J. Geophys. Res. Biogeosciences*, 113 (G0403, 1–11, doi:10.1029/2008JG000689, 2008.
- 725 Saurer, M., Kress, A., Leuenberger, M., Rinne, K. T., Treydte, K. S. and Siegwolf, R. T. W.: Influence of atmospheric circulation patterns on the oxygen isotope ratio of tree rings in the Alpine region, *J. Geophys. Res. Atmos.*, 117(5), doi:10.1029/2011JD016861, 2012.
- Saurer, M., Spahni, R., Frank, D. C., Joos, F., Leuenberger, M., Loader, N. J., Mccarroll, D., Gagen, M., Poulter, B., Siegwolf, R. T. W., Andreu-Hayles, L., Boettger, T., Dorado Liñán, I., Fairchild, I. J., Friedrich, M., Gutierrez, E., Haupt, M., 730 Hilasvuori, E., Heinrich, I., Helle, G., Grudd, H., Jalkanen, R., Levanič, T., Linderholm, H. W., Robertson, I., Sonninen, E., Treydte, K., Waterhouse, J. S., Woodley, E. J., Wynn, P. M. and Young, G. H. F.: Spatial variability and temporal trends in water-use efficiency of European forests, *Glob. Chang. Biol.*, 20(12), doi:10.1111/gcb.12717, 2014.
- Seager, R., Hooks, A., Williams, A. P., Cook, B., Nakamura, J. and Henderson, N.: Climatology, variability, and trends in the U.S. Vapor pressure deficit, an important fire-related meteorological quantity, *J. Appl. Meteorol. Climatol.*, 54(6), 735 doi:10.1175/JAMC-D-14-0321.1, 2015.
- Simmons, A. J., Willett, K. M., Jones, P. D., Thorne, P. W. and Dee, D. P.: Low-frequency variations in surface atmospheric humidity, temperature, and precipitation: Inferences from reanalyses and monthly gridded observational data sets, *J. Geophys. Res. Atmos.*, 115(1), doi:10.1029/2009JD012442, 2010.
- Slivinski, L. C., Compo, G. P., Whitaker, J. S., Sardeshmukh, P. D., Giese, B. S., McColl, C., Allan, R., Yin, X., Vose, R., 740 Titchner, H., Kennedy, J., Spencer, L. J., Ashcroft, L., Brönnimann, S., Brunet, M., Camuffo, D., Cornes, R., Cram, T. A., Crouthamel, R., Domínguez-Castro, F., Freeman, J. E., Gergis, J., Hawkins, E., Jones, P. D., Jourdain, S., Kaplan, A., Kubota, H., Blancq, F. Le, Lee, T. C., Lorrey, A., Luterbacher, J., Maugeri, M., Mock, C. J., Moore, G. W. W. K. K., Przybylak, R., Pudmenzky, C., Reason, C., Slonosky, V. C., Smith, C. A., Tinz, B., Trewin, B., Valente, M. A., Wang, X. L., Wilkinson, C., Wood, K. and Wyszyński, P.: Towards a more reliable historical reanalysis: Improvements 745 for version 3 of the Twentieth Century Reanalysis system, *Q. J. R. Meteorol. Soc.*, 145(724), 2876–2908, doi:10.1002/qj.3598, 2019.
- Treydte, K., Schleser, G. H., Esper, J., Andreu, L., Bednarz, Z., Berninger, F., Böttger, T., D’Alessandro, C. D., Etien, N., Filot, M., Frank, D., Grabner, M., Gutierrez, E., Haupt, M., Helle, G., Hilasvuori, E., Jungner, H., Kalela-Brundin, M., Leuenberger, M., Loader, N., Masson-Delmotte, V., Pazdur, A., Planells, O., Pukiene, R., Reynolds, C., Rinne, K., 750 Saurer, M., Sonninen, E., Stievenard, M., Switsur, R., Szczepanek, M., Todaro, L., Waterhouse, J., Weigl, M. and Wimmer, R.: Climate signals in the European isotope network ISONET, *Tree rings Archaeol. Climatol. Ecol. TRACE*, 5, 138–147, 2007a.
- Treydte, K., Frank, D., Esper, J., Andreu, L., Bednarz, Z., Berninger, F., Boettger, T., D’Alessandro, C. M., Etien, N., Filot, M., Grabner, M., Guillemain, M. T., Gutierrez, E., Haupt, M., Helle, G., Hilasvuori, E., Jungner, H., Kalela-Brundin, 755 M., Krapiec, M., Leuenberger, M., Loader, N. J., Masson-Delmotte, V., Pazdur, A., Pawelczyk, S., Pierre, M., Planells,



- O., Pukiene, R., Reynolds-Henne, C. E., Rinne, K. T., Saracino, A., Saurer, M., Sonninen, E., Stievenard, M., Switsur, V. R., Szczepanek, M., Szychowska-Krapiec, E., Todaro, L., Waterhouse, J. S., Weigl, M. and Schleser, G. H.: Signal strength and climate calibration of a European tree-ring isotope network, *Geophys. Res. Lett.*, 34, L24302(24), 1–6, doi:10.1029/2007GL031106, 2007b.
- 760 Trigo, R. M., Vaquero, J. M., Alcoforado, M. J., Barriendos, M., Taborda, J., García-Herrera, R. and Luterbacher, J.: Iberia in 1816, the year without a summer, *Int. J. Climatol.*, 29(1), doi:10.1002/joc.1693, 2009.
- Tyralis, H., Papacharalampous, G. and Langousis, A.: A brief review of random forests for water scientists and practitioners and their recent history in water resources, *Water (Switzerland)*, 11(5), doi:10.3390/w11050910, 2019.
- Vitas, A.: Tree-ring chronology of Scots pine (*Pinus sylvestris* L.) for Lithuania, *Balt. For.*, 14(2), 2008.
- 765 Volcano World: Laki, Iceland - 1783, Oregon State Univ. [online] Available from: <https://volcano.oregonstate.edu/laki-iceland-1783> (Accessed 24 February 2023), 2023.
- Willett, K. M., Dunn, R. J. H., Thorne, P. W., Bell, S., De Podesta, M., Parker, D. E., Jones, P. D. and Williams, C. N.: HadISDH land surface multi-variable humidity and temperature record for climate monitoring, *Clim. Past*, 10(6), doi:10.5194/cp-10-1983-2014, 2014.
- 770 Williams, A. P., Allen, C. D., Macalady, A. K., Griffin, D., Woodhouse, C. A., Meko, D. M., Swetnam, T. W., Rauscher, S. A., Seager, R., Grissino-Mayer, H. D., Dean, J. S., Cook, E. R., Gangodagamage, C., Cai, M. and Mcdowell, N. G.: Temperature as a potent driver of regional forest drought stress and tree mortality, *Nat. Clim. Chang.*, 3(3), doi:10.1038/nclimate1693, 2013.
- Yang, J., Jiang, L., Luo, J., Pan, J., Lemmetyinen, J., Takala, M. and Wu, S.: Snow depth estimation and historical data reconstruction over China based on a random forest machine learning approach, *Cryosphere*, 14(6), doi:10.5194/tc-14-1763-2020, 2020.
- 775 Yuan, W., Zheng, Y., Piao, S., Ciais, P., Lombardozzi, D., Wang, Y., Ryu, Y., Chen, G., Dong, W., Hu, Z., Jain, A. K., Jiang, C., Kato, E., Li, S., Lienert, S., Liu, S., Nabel, J. E. M. S., Qin, Z., Quine, T., Sitch, S., Smith, W. K., Wang, F., Wu, C., Xiao, Z. and Yang, S.: Increased atmospheric vapor pressure deficit reduces global vegetation growth, *Sci. Adv.*, 5(8), doi:10.1126/sciadv.aax1396, 2019.
- 780 Zhan, Y., Luo, Y., Deng, X., Grieneisen, M. L., Zhang, M. and Di, B.: Spatiotemporal prediction of daily ambient ozone levels across China using random forest for human exposure assessment, *Environ. Pollut.*, 233, doi:10.1016/j.envpol.2017.10.029, 2018.
- Zhao, C., Liu, B., Piao, S., Wang, X., Lobell, D. B., Huang, Y., Huang, M., Yao, Y., Bassu, S., Ciais, P., Durand, J. L., Elliott, J., Ewert, F., Janssens, I. A., Li, T., Lin, E., Liu, Q., Martre, P., Müller, C., Peng, S., Peñuelas, J., Ruane, A. C., Wallach, D., Wang, T., Wu, D., Liu, Z., Zhu, Y., Zhu, Z. and Asseng, S.: Temperature increase reduces global yields of major crops in four independent estimates, *Proc. Natl. Acad. Sci. U. S. A.*, 114(35), doi:10.1073/pnas.1701762114, 2017.
- 785